KERNFORSCHUNGSZENTRUM

KARLSRUHE

November 1976 KFK 2378

Institut für Reaktorentwicklung
Projekt Schneller Brüter

Sodium Boiling Experiments in a 7-Pin Bundle under Flow Rundown Conditions

J. Aberle, A. J. Brook, W. Peppler
H. Rohrbacher, K. Schleisiek

GESELLSCHAFT
FÜR
KERNFORSCHUNG M.B.H.

KARLSRUHE

GESELLSCHAFT FÜR KERNFORSCHUNG M. B. H.

KARLSRUHE

KERNFORSCHUNGSZENTRUM KARLSRUHE

Institut für Reaktorentwicklung
Projekt Schneller Brüter

KFK 2378

Sodium Boiling Experiments in a 7-Pin Bundle under Flow Rundown Conditions

J.Aberle
A.J.Brook *
W.Peppler
H.Rohrbacher
K.Schleisiek

*) United Kingdom Atomic Energy Authority, Risley

Gesellschaft für Kernforschung mbH., Karlsruhe

Erratum

Page 12, first line. 0.1 should read 0.35

Page 17, last sentence. 74% should read 58%

Summary Table, Test 27. Channel Inlet Pressure at t_B should be 1.73, and Total Pressure Drop at t_B should be 0.68 bar.

Addendum

The incidence of re-wetting following the re-establishment of forward flow after the termination of flow reversal is mentioned in this report. Since preparation of the report, it has been pointed out that the converse is also true, i.e. that dryout begins shortly after the start of flow reversal. Although reversal does not necessarily lead to dryout, dryout is only to be found following reversal, and the time delay between the start of these two events is remarkably constant, in the range 0.18 to 0.27sec. It is also notable that unless the transition to annular flow has already occurred (which it has in a few instances) the time of transition also corresponds to the onset of flow reversal. This results from downward flow forcing the lower liquid column into cooler regions, thereby suppressing further nucleations. This is the converse of the mechanism described in the report for the upward moving lower column, and therefore quite consistent with it. The establishment of an annular flow regime and the absence of further nucleations below the vapour result in no further replenishment of the liquid film and consequently the onset of dryout. The interval between the starts of flow reversal and dryout enables an evaluation to be made of the instantaneous value of liquid film thickness. This is estimated to be in the range 0.08 to 0.15mm, which is in good agreement with previously published values. It seems clear that the incidence of flow reversal may be the most dominant single factor in the occurrence of dryout.

Abstract

A series of experiments has been carried out using an electrically heated seven pin bundle to simulate the conditions under which boiling of the sodium coolant could occur in the event of the loss of electrical supplies to the circulator pumps of a fast reactor, coincident with a failure of the reactor to trip.

Although it was not possible to represent the conditions of the reactor exactly, nor to continue the tests far into dryout, the results nevertheless give valuable qualitative information on the course of boiling development as well as useful quantitative information against which the predictions of computer codes such as BLOW 3 can be checked. In particular, data was obtained relating to the incidence of superheat, the location and time to dryout of the residual liquid films, the void fraction within the boiling region, and the types of flow regimes which may be expected within different parts of the boiling region at various stages of the transient.

Na-Siedeexperimente in einem 7-Stab-Bündel zum Kühlmitteldurchsatz-Störfall

---

Zusammenfassung

In einem elektrisch beheizten Siebenstabbündel wurden experimentelle Untersuchungen zum Ablauf von Natriumsiedevorgängen in Brennelementen Schneller Brutreaktoren bei Ausfall der Kühlmittelpumpen und gleichzeitigem Versagen der Reaktor-Schnellabschaltung untersucht.

Obwohl es nicht möglich war, die Reaktorbedingungen exakt einzustellen, und die Vorgänge bis über das Auftreten von Dryout hinaus zu verfolgen, liefern die Versuche dennoch wesentliche qualitative Informationen zum Ablauf von Siedevorgängen in Stabbündel-Anordnungen. Die quantitativen Ergebnisse werden zu einer Überprüfung von Computer-Codes wie z.B. BLOW 3 herangezogen. Weitere Versuchsergebnisse betreffen das Auftreten von Siedeverzug, den Zeitpunkt und Ort des Auftretens von Dryout (vollständiges Abdampfen des Flüssigkeits-Restfilms), den Blasenvolumenanteil im Siedebereich sowie die Strömungsformen in den einzelnen Siedebereichen zu verschiedenen Zeitpunkten der transienten Siedevorgänge.

Contents

1. INTRODUCTION

The possibility of coolant boiling raises important questions in connection with fast reactor safety [1]. Liquid metals differ from more normal fluids in a number of respects, such as high thermal conductivity and good wetting properties, and it might, therefore, be expected that their boiling behaviour too differs from fluids such as water. A number of sodium boiling experiments have been carried out at various institutions, but until recently these were carried out exclusively in simple test sections of cylindrical or annular cross section.

A series of 157 boiling experiments has recently been concluded in GfK Karlsruhe in which groups of seven heater pins within hexagonal wrappers served to represent the fuel pins within a fast reactor subassembly. The subject of this report is the group of ten experiments in which a simulation was made of a failure of the electrical supply to the pumps of a fast reactor, coupled with a coincidental failure of the reactor to trip. The experiments formed a part of the safety R and D work which is being carried out in support of the SNR 300 FBR development, and were undertaken using the second of the seven pin bundles in the Karlsruhe NSK loop.

The primary aim was of course to ascertain the course of transient boiling under pump rundown conditions: of particular interest are the location of the void and its rate of growth, the incidence of dryout of the liquid films, which leads to the loss of heat transfer from the pin surface, the incidence of superheat, and the possibility of inlet flow reversal and hydrodynamic instability. The experiments served also as a test of heater pins under transient conditions, this aspect being of particular relevance to local blockage experiments currently being prepared.

Although the work was carried out in support of SNR development, it is important to realize the limited extent to which the bundle was representative of the SNR subassembly. In particular, it should be noted that although the pin pitch and diameter and, therefore, the hydraulic diameter of the subchannels corresponded to those

of the fuel element, the length of the heated section was only 600 mm, compared with a fuelled length of 950 mm for the SNR core, and the axial power distribution was linear rather than chopped cosine. (The length of the upper, unheated section, on the other hand, 455 mm, compared well with that of the upper axial breeder in SNR.) The differences made it necessary for some of the test parameters to be adjusted to special values before the transient was initiated, so that the axial temperature and pressure profiles shortly before the onset of boiling became as similar as possible to those calculated for a typical SNR subassembly. A simple single phase transient calculation resulted in the choice of parameters listed in the upper part of the Summary Table which is to be found at the back of this report. With these combinations of values, the axial temperature profiles at the onset of boiling correspond reasonably well to those in the SNR fuel element, although there are some discrepancies. The principal of these arises from the linear power distribution in the heater pins, which produces the maximum temperatures at the top end of the heated section. In the SNR element, the cosine power distribution gives a temperature maximum in the upper third of the fuelled zone. Likewise, the axial temperature profile is somewhat steeper in the seven pin bundle than in the fuel element, but it is not believed that these differences can seriously influence the test results. Perhaps of greater importance is the marked radial temperature profile across the bundle, and the relatively greater influence of the wrapper wall, the thermal capacity of which amounted to 28 % that of the whole bundle.

2. TEST SECTION AND INSTRUMENTATION

The test section is illustrated in Fig.1. The seven pins of 6 mm o.d. lie on a 7.9 mm pitch, surrounded by a hexagonal wrapper and supported by spacer grids, the separation of which corresponds to the SNR fuel bundle. At the upper end, pin geometry is preserved into the unheated region, which simulates the upper axial blanket. This unheated blanket extends a distance of 455 mm: above it the hexagonal wrapper is retained for a further 170 mm, beyond which the cross section becomes circular. The upper mixing

chamber is positioned 925 mm from the upper end of the heated section. At the lower end of the test section is the sodium inlet; coolant enters into a small chamber and passes downwards before reversing into an unheated entry length of some 80 mm. Power supply to the pins also comes in from below, electrical return being via the heater pin sheath, coolant, grids and hexagonal wrapper. A throttle valve is mounted on the inlet pipe, and beyond this is the junction with the flow bypass, which rejoins the test section in the upper mixing chamber.

Fig.1 also illustrates the location of the test section instrumentation. This consisted of

a) a total of some forty thermocouples. The locations of these are identified in Fig.1 (as TE1 etc), but for clarity the positions are summarized in Table 1 below.

TABLE 1

Second Seven Pin Bundle: Thermocouple Locations

Level (mm)	Central Coolant Channel	Edge Coolant channel	Centre Pin	Edge Pin Inner Sector	Edge Pin Middle Sector	Edge Pin Outer Sector	Wrapper
1300							40
1100							39
1000	12			(37)	38		
850	11			35	36		
700	9	10	32		34	33	17
580	7	8	25	30	27	26	16
				(28)		(29)	
						(31)	
500	6			22	23	24	
400	4	5	(20)		21		15
250	3			19		18	

( ) denotes thermocouple was faulty.

In addition to those indicated, T_1 and T_2 were mounted in the inlet leg, measuring coolant temperature, and T_{13} recorded temperatures within the mixing/condensation chamber at the top end. T_{14} monitored the wall temperature of the lower inlet chamber.

The heater pin thermocouples were of chromel/alumel, mineral insulated, in a stainless steel sheath,and were only 0.25 mm diameter. They were attached by brazing into grooves cut into the outer wall of the heater pins. Coolant thermocouples were 0.5 mm diameter, and entered the test section through the wrapper wall, to which their supports were attached.

b) Permanent magnet flow meters monitoring the inlet and outlet flows to and from the test section, and through the bypass. Integration and differencing of the signals received from these enabled the axial extent of the equivalent void to be ascertained once boiling had begun.

c) Five Chen type bubble detectors [2], mounted at 4 different levels. Two detectors mounted at the 500 mm level were positioned in a central and an edge subchannel; the remainder all in the central channels. These are represented by the letter C in Fig.1.

d) Six Jodel type void detectors, J1 - J6. This type of instrument measures electrical resistivity across the test section, an increase in resistance being attributable to the presence of vapour. Although early experience with this type of instrument in single channel geometry had been successful, in this more advanced type of test section, these detectors failed to yield meaningful signals.

e) Two pressure transducers P0 and P2 measuring absolute pressure at the end of the heated section, and on the inlet side upstream of the throttle valve, respectively.

f) Four piezo-electric pressure transducers, P3 to P6 in Fig.1, to monitor rapid pressure fluctuations.

g) Four inductive KAMAN transducers, S1 - S4, also to monitor dynamic pressures.

h) Two piezo-electric acoustic sensors, A1 and A2, in conjunction with appropriate acoustic waveguides, and a piezo-electric microphone S5 mounted over the mixing chamber.

The arrangement of the pressure and acoustic transducers in the bundle is represented in Fig.2.

For temperature decoupling of the inductive and piezo electric pressure transducers, short sodium filled stubs were used, which were provided with controlled trace heating. This ensures that the rapid temperature changes occurring during the tests did not exert noticeable influence on the pressure measurement system.

In some measurement planes different types of sensors were provided to ameliorate the interpretation of the measurement results in case of different transfer function of the sensors. The bandwidth of the pressure transducers and the associated measuring chains was 20 kHz.

Since the diaphragms of the pressure transducers were in direct contact with the sodium, both pressure transducers remained largely unaffected by the forces of acceleration appearing in the cladding tube structure. Their transmission characteristics were linear up to 5 bars.
The two accelerometers (A1 and A2) had a bandwidth of 70 kHz, and the piezo-electric microphone, with compensated acceleration (S5) had a response of 40 kHz.

Fig.3 shows a block diagram of the data acquisition and processing chain. The signals coming from the individual sensors were transmitted via preamplifier and decoupling amplifiers. Undergrounded, electrically decoupling amplifiers were used in order to avoid disturbing influences. Magnetic tape units and visicorders as well as a digital data acquisition system with multiplexer inputs were utilized in data recording. The digitized measured values were

processed on an IBM computer and subsequently evaluated and plotted as time dependent physical units, auto-power and cross-power spectral densities, respectively. In addition, the power spectrum of measured data stored on the analog tape is obtained by means of an additional spectral analyzer.

For the production of the illustrations of void development described later in this report, the Chen detectors, thermocouples and flow meters were of primary importance, and it is perhaps appropriate to comment on the usefulness of these items and on their limitations.

To begin with the Chen detectors, these were found to give clear and unequivocal signals of the presence of vapour, and had a rapid response time. It is unfortunate that they were present only at four levels, 250, 500, 700 and 850 mm, particularly in view of the failure of the Jodel type monitors to deliver decipherable signals, since they clearly define the bounds of the boiling region. Moreover, study of the Chen records give good indication of the form of the flow regime, e.g. bubbly/homogeneous, annular or plug type of flow, all of which were found in various stages of the transient. They are, however, insufficiently sensitive to reveal the small droplets present in annular mist flow.

The thermocouples were useful in indicating the presence of boiling conditions between and beyond the positions of the Chen probes, but care had to be taken in their interpretation to deduce the presence of vapour, since no distinction can be made between vapour and liquid at the same temperature. The way in which these signals varied was of rather greater value than their absolute level. For instance a rapid coming together of temperatures at two radial positions at the same axial height must indicate the presence of vapour; the reduction in temperature of a point at or below the saturation level suggests the presence of cold liquid, or rapid reduction from a level above saturation suggests the rapid generation of vapour, particularly when accompanied or immediately preceded by a change in pressure or flow velocity. An increase in the rate of temperature rise can be associated with the condensation of vapour, and this may be con-

firmed at those levels where Chen detectors are also stationed; such changes in gradient soon become recognisable. The thermocouples seem to be of least use during the collapse phase when the liquid adjacent to the boiling interface is hot and when axial temperature gradients in the coolant are relatively low. Comparison with the Chens suggests that the effective time delay before the temperature was significantly decreased, was in some tests as much as 0.05 to 0.1 second.

The flow meters on inlet and outlet legs of the test section enabled the times of the start of boiling and of bubble collapse to be precisely determined, particularly when used in conjunction with the pressure records and, of course, to ascertain the incidence of flow reversal. By integration of the signals, it was possible to determine the "equivalent void", i.e. the length which would be occupied by the vapour region, were its void fraction 100 %. Care must be taken over this integration, for several reasons, which include the changes in cross section of the flow area, errors arising from the passage of vapour through the outlet flow meter, and an apparent, possibly transient, dependency of the signal received upon the temperatures of the coolant and of the meter. Although these errors are hardly significant in the measurement of flow velocity, integration over several seconds can compound the discrepancy, so that at the time of vapour collapse, the upper and lower vapour interfaces appear to be no longer coincident. In practice this proved to be easily, if perhaps a little arbitrarily, taken into account by adjustment of the baseline, and it seems unlikely that errors of more than a few percent were introduced in this way.

The position of the equivalent void on the plots described later is completely arbitrary. They have been drawn so as to fit reasonably well within the boiling envelope, but any part of the curves may be moved up or down, provided the separation between them is maintained. All that can be said is that, during periods of flow reversal, the lower curve must move down by an amount at least that by which the lower liquid column moves down. This information comes, of course, from the inlet velocity measurement

integrated over the period for which it is negative. The boiling boundary may move downwards more or less than this amount: in the curves, it too, moves by at least this value.

3. TEST RESULTS

3.1 General Notes

In the notes which follow, the results of two of the tests will be described in detail, the remainder somewhat more briefly, and an attempt is made to consider the influence of the various parameters, in so far as this is possible, by a comparison of the results from the different tests.

Before doing this, one point must be made concerning the representation in the Figures of the boiling region and the equivalent void. Although these appear at first glance to be somewhat akin in general form to the bubble growth patterns predicted by, e.g. the BLOW 2 code, the similarity is no more than this, since the envelope of the boiling region encompasses a zone in which multi-bubble boiling, with the full range of normal two phase flow features, is taking place. They may, therefore, be, and often is, a considerable fraction of this region occupied by liquid. This contrasts with the single vapour bubble model of BLOW 2, through which no liquid mass transfer takes place.

Secondly, for comparative purposes, much reference is made to the Summary Table in which many features of the results are recorded. Some points in connection with this Table must be made.

a) Channel outlet pressure refers to the pressure in the mixing chamber.

b) Channel inlet pressure is measured in the inlet leg upstream of the throttle valve.

c) The time at which boiling begins is taken as that at which the first clear signal is received, even though vapour location may not be known, and even though a significant time may elapse before continuous void growth is attained.

d) Dryout does not begin always at the same level. The time recorded is that at which the earliest signal is received: further data can be obtained from the figures.

e) The time at which boiling ceases is normally taken as the time of final collapse of the largest void.

f) In Test 28, the pump was switched off, and the throttle valve closed rapidly.

Furthermore, in connection with the Figures, the representation of a long period of dryout - by means of a horizontal line at the appropriate level - does not necessarily mean that continuous dryout occurred at some location at that level; only that some point or another was suffering dryout throughout that period. Continuity is only apparent because of the overlapping of the lines.

3.2 Test 7-2/16

In Figs.4 to 12 appear some of the records obtained from this test, along with the transient form of the boiling region and the equivalent void.
At nucleation, the main test conditions were:

- Flow velocity	1.13 m/sec
- Pressure drop	0.57 bar
- Heat flux	150.3 W/cm^2
- Throttle valve	Intermediate

The flow transient was initiated some three seconds after recording began, and boiling started 9.15 seconds later. There was no evidence of any superheat. Saturation temperature was reached first, as in all tests with the 7 pin bundles, in the central subchannels. The absence of superheat and consideration of the axial temperature profile (Fig.12) suggests that boiling begins at or close to the end of the heated section. Initially, only small vapour bubbles are generated, which condense again. This is shown by the very small fluctuations in outlet flow signal (Fig.6) and

by the peaks in the dynamic pressure records (Fig.8). Because of the throttling effect, feedback to the inlet flow is still small in these early stages.

Void development is rather slow as long as saturation temperatures do not extend over the whole cross section. To demonstrate better the course of events during this early phase, results obtained during the first 1.35 seconds of the run are plotted together on a larger time scale in Fig.5. In this diagram, the development of the equivalent void and the boiling region are reproduced, as deduced from the Chen detectors and temperature recordings. With the aid of these and the flow signals, integrated as necessary, the pulsating radial growth of the vapour region was estimated. The significant phases are drawn in the cross sections (a) to (i), below which the length L and diameter d of the bubble are recorded.

Integration of the flow signals reveals a very small bubble (a) which nucleates at 12.15 and collapses at 12.26 sec (b). The next bubble has an equivalent length which is a maximum of 8 mm at 12.3 sec. This corresponds to a bubble radius of about 8 mm or the central subchannels voiding over a length of 26 mm. Pressure records show that this bubble collapses too, at 12.37 sec, although there remains some voidage in the channel: presumably some other new bubble is also present. This last collapse is followed by further pulsations in the outlet flow, until at 0.55 sec after the onset of boiling in the central subchannels, saturation temperature is attained by the outer subchannels. Even at this time (12.7 sec - phase (i)), the wrapper wall temperature lies somewhat below saturation, not reaching 930 ^{o}C until 13.4 sec. This is the result of the high heat capacity of the wrapper.

Once boiling temperatures are attained throughout the cross section, from 12.7 seconds, the void grows with increasing velocity into the heated section and into the upper unheated section which simulates the axial breeder of the reactor. The pulsations of the outlet flow become progressively more violent until at 13.9 seconds, flow reversal on the inlet side is found to occur (Fig.6). This flow reversal persists until 14.26 seconds,at which time the pres-

sure drop across the test section is only 0.1 bar. Towards the end of this flow reversal, power was switched off, because of the onset of dryout.
During this growth phase, the equivalent void is about two thirds the size of the boiling region, i.e. the boiling region is about one third liquid, two thirds vapour. The distribution of vapour within the region can be deduced from the Chen signals, which clearly indicate a high liquid fraction for the half second or so following their first registering the presence of vapour, i.e. the liquid content is high close to the boiling boundary. Later, when the boiling region has extended well beyond these Chens, they indicate only the presence of vapour, i.e. an annular flow regime, in which any liquid present lies largely on the surface of the heater pins.

During this time, the axial temperature distribution is essentially flat throughout the boiling region (Fig.12), exactly as would be expected. At 14.1 seconds, the time at which the first dryout signals were received, the boiling region extends from about 300 to 1000 mm: at the lower end the temperature is about 945 ^{o}C, and at the upper, about 925 ^{o}C. This corresponds to a pressure drop in the two phase mixture of 0.27 bar, but it would be unwise to draw conclusions from this, because of the transient conditions. (The inlet temperature to the test section at this time is not shown in Fig.12, since an inlet flow reversal is in progress, and inlet temperature was measured in the inlet leg to the test section.)

Saturation temperatures are reached at the different axial levels in the order 580, 500, 700, 850, 400, 1000 and 250. The thermocouple at the 250 mm level (T3) clearly indicated saturation temperatures (Fig.10) but no signal was received from the Chen detector. This is probably explained by asymmetry resulting from finite tolerances in the construction of the test section, or from bowing of the heater pins, since the thermocouple and the Chen detector were positioned on opposite sides of the central pin.

The first dryout signals were received at 14.13 seconds, 1.98 seconds after the first indications of boiling, and power supply was terminated .08 seconds later. Some thermocouple records illustrating dryout appear in Fig.9. It is interesting to note that at the very same time that dryout was first indicated on the central pin (T25 at 580 mm), dryout signals were also received from T26 which is situated at the same level on one of the outer pins facing outwards towards the wrapper wall. This is in spite of the fact that boiling in the wall subchannels started 0.55 seconds later than in the central subchannels. Only .07 seconds later, two other thermocouples, T27 and T30, indicated dryout. These are situated on the central and inner sectors of the outer pins respectively. It is, therefore, clear that dryout occurs at almost the same time across the whole of the cross section at the 580 mm level. Shortly after power switch off, dryout is also found at the 500 mm measuring plane - a consequence of continuing heat conduction from the centre of the pins.

Following power switch off, the vapour region enters a partial collapse phase of the oscillation (14.4 seconds), before pulsating outwards again and causing a second reversal of the inlet flow (14.46 - 14.68 seconds); the consequent collapse is initially fairly rapid (at least that of the equivalent void), and subsequently slower until collapse is completed at 16.26 seconds (Fig.4). The first of these partial collapses causes re-wetting of the dried out clad at 500 mm, even though the boiling interface remains well below this level. The rapid phase of the second collapse similarly causes re-wetting at 580 mm, even though this level is almost at the centre of the boiling region.

Following the transmission of the conduction wave through the heater pin after power supply termination, there is a clear change in the nature of the Chen detector signals (Fig.7), which now indicate what is apparently a plug flow type of flow regime. Since there is little energy available to evaporate the residual film, the liquid plugs between the vapour bubbles pass upwards through the boiling region without losing liquid to the heater pin surfaces, and since vapour transport rates must be lower, there is no tendency to the development of annular flow.

A point should be made about the heat flux to the wrapper wall. At the 580 mm level, this is about 23 w/cm^2 during the single phase flow transient: this corresponds to a rate of temperature rise of 46 ^{o}C/second. During vapour growth, it increases to a maximum of about 44 w/cm^2, or about 90 ^{o}C/second.

To give a distinct picture of the variation of the radial temperature profile, temperature values for the 580 mm measuring plane at times of 12.15, 12.7 and 13.1 sec. are shown in Fig.11. At the onset of boiling there is a temperature difference of 67 ^{o}C between the wrapper wall and the central pin (or the central subchannels). At 12.7 seconds, the edge channels too have reached saturation temperature, and the temperature drop across the test section has decreased to 37 ^{o}C. At 13.1 seconds, this difference has decreased further to only 17 ^{o}C, much of which can be accounted for by the difference in temperature between the inner wall surface and the thermocouple, which is mounted in a groove 0.6 mm deep in the outside of the 1.5 mm thick wall.

3.3 Test 7-2/24 (Figs.13 - 20)

The highest level of superheat found in these tests occurred in Test 7-2/24, where a value of 68 ^{o}C was measured.At the onset of boiling, the coolant in the central subchannels was above saturation temperature over a length of 180 mm (Fig.20). This directly measured value is confirmed by the pressure pulse of 0.9 bar which occurred at the onset of boiling.

The important test conditions when boiling began were

flow velocity	0.33 m/sec
pressure drop	0.21 bar
heat flux	99.3 w/cm^2
throttle valve	fully open

Remarkable differences were found between the results of this test and those of, e.g. 7-2/16 described earlier. Immediately at the onset of boiling, at 9.87 sec, a vigorous expulsion took place

(Fig.13), probably originating from a location between 520 and 540 mm. Because of the high superheat a high pressure pulse (Fig.16) was generated which was about four times greater than the remaining pressure drop from the pump rundown. Flow reversal at channel inlet, therefore, took place almost instantaneously (Fig.14). Thus, from the very start of boiling, the system was in an unstable condition.

The initial expulsion is followed by partial collapse and a series of subsequent oscillations (Fig.13). These are very clearly defined from the Chen signals, pressure fluctuations, flowmeters and by some thermocouples (Figs.14 to 18). The frequency of these oscillations is initially about 2.2 Hz, decreasing later to 1.5 Hz or less. The amplitude of oscillation of the upper sodium column amounts to about 200 mm; that of the lower is typically 100-150 mm. The equivalent void varies in a manner which closely matches changes in the pattern of the boiling region, and suggests that only relatively small quantities of liquid are present in the vapour. This appears to be confirmed by the very square-cut form of the Chen signals (Fig.15), e.g. C4 at 700 mm between 10 and 13 seconds, which indicates an absence of liquid entrainment close to the upper interface. However, the vigorous oscillations produce the effect that during re-entry, some droplets of liquid penetrate deeply into the test section. This is indicated by the signals from the Chen detectors at the 500 mm level; C3 in the central subchannel at 10.2 sec, and C2 in an outer subchannel at 10.2 and 10.6 sec.

The radial temperature profile very rapidly disappears after the onset of boiling (Fig.19). For instance, at the 580 mm level, thermocouples 25 (centre pin) and 26 (outer pin facing the wrapper) come together within 100 msec of vapour appearing at the centre pin. This compares with the 550 msec found in test 7-2/16. Axially, the superheat above saturation temperature disappears completely during the first expulsion, as will be seen from Fig.20, where the axial temperature distribution at 10.1 sec is illustrated. The small residual energy excess which appears to remain at one location (T22) in the heater pin wall is in fact caused by a temporary dryout.

Within 130 msec of its emergence into vapour (some 70 msec or so after nucleation at 9.94 sec) this one thermocouple (T22) at the 500 mm level experiences a dryout (Fig.17). In the 130 msec which passes before its rewetting at 10.2 sec, there is an increase in indicated temperature of 33 ^{o}C. Such a rapid increase is characteristic of dryout. At the 400 mm level, T21 experiences a similar temporary dryout between 10.5 and 10.6 seconds. Dryout without rewetting begins between 10.4 and 10.5 seconds at the 500 and 580 mm measuring planes, about 0.5 sec after the first temporary dryouts. After a further 0.5 sec, T21 in the 400 mm plane also dries out permanently. Thus within one second of the onset of boiling, extended regions of the bundle are no longer cooled. Power supply was terminated at 11.2 sec.

In Fig.20 the temperature profiles for three different times are plotted. A distinction must be made between the central and the wall subchannels. In contrast to test 7-2/16, in this test even the coolant in the outer subchannels reaches saturation temperature at the top of the heated section. At the time of nucleation, there is a 90 ^{o}C temperature drop from the central pin to the wrapper, and about 60 ^{o}C between the central and outer subchannels. This radial variation decreases in the upper unheated section, largely disappearing by the 1000 mm measuring plane.

By 10.1 sec, shortly after the maximum of the first ejection, temperatures are equalised both axially and radially throughout the boiling region (350 to 750 mm), and the thermocouples which hitherto showed superheat, now indicate the lower saturation temperature. At the time power is switched off at 11.2 sec, the vapour extends from about 200 to about 670 mm and there is ready evidence of dryout. Thermocouples at 250 and 580 mm are still cooled by remaining droplets or slugs of liquid or by rewetting during the liquid oscillations.

3.4 Reproducibility

With such a small number of experiments, it is clearly important that reproducibility should be established before conclusions are reached on the influence of the various parameters, some of which

e.g. superheat, may be outside experimental control. In this respect it is worthwhile to compare the results of Tests 14 and 25, and Test 17 with Test 27.

Taking the first pair, 14 and 25, it will be seen that the general appearance of the early part of the voiding curves (Figs.21 and 22) is very similar. The Summary Table quantifies the similarity. It will be seen that up to the time of power switch off, i.e. in the first two seconds or so, the pattern of void development in the two cases is very similar, differences in axial extent, time to dryout or flow reversal, etc. differing by no more than 12 % when measured from the time of nucleation. The rather slower rate of growth of the vapour region in Test 25 is consistent with the slightly higher pressure in the channel at this stage.

The principal differences between the cases are largely a consequence of the later power switch off in Test 25. In Test 14, the power supply to the pins was terminated shortly after inlet flow reversal was indicated, and before dryout, although dryout signals were received from the 580 mm level shortly afterwards - a consequence of continued conduction through the pin as temperatures equalised. The second test, 25, relied upon automatic tripping of the power supply as a consequence of dryout signals being received: dryout was, therefore, more widespread at the 400, 500 and 580 mm levels, and vapour extended right into the upper condensation plenum before power was switched off. It is of interest to note again that rewetting of these dried out zones occurred in each case following a rise in the position of the lower boiling boundary. The irregular behaviour of the outlet flowmeter (V3) once it is reached by vapour is clearly demonstrated in Fig.22.

Tests 17 and 27 were carried out under conditions which were not quite so alike as those of 14 and 25. The principal difference lay in the lower inlet temperature of Test 17, which would increase the time to the start of boiling, but which was partially compensated for by the rather more rapid rate of fall of the pressure drop. The pressure drop and flow velocity at the time boiling begins was significantly higher in Test 27 - by about 74 % and 52 % respectively.

As a result of this, the vapour extends downwards more slowly, and upwards more rapidly, in the later test (see Figs.23 and 24). The overall rate of void development during the first major growth phase was greater in Test 27, but in general the values tabulated in the lower part of the Summary Table agree within about 30 %.

The major differences between this pair of results again arises in the later part of the transient following power shut off; this was later in the second test, during which vapour again extended into the condensation chamber. The effect of this on the outlet flowmeter is once again clearly seen (Fig.24).

3.5 Influence of Main Parameters

The influence of a higher system pressure can be seen by comparing the results of Test 16 (Fig.4) with those of 14 and 25 (Figs.21 and 22). The steady state flow velocities and inlet temperatures are essentially the same, as are the pressure drops, throttle valve settings, heat fluxes, and rates of pressure decrease. Because of the higher pressure, boiling begins a little later in Test 16, when the pressure drop and flow velocity is a little lower: superheat is still zero. The rate of growth of both the equivalent void and the boiling region are essentially the same as in the two lower pressure cases, but there is a clear tendency for the void to remain lower in the channel, the lower interface reaching 300 mm more rapidly, and the upper one reaching 850 mm more slowly than in the two other cases - a consequence of the lower pressure drop, although flow reversal occurred at about the same time as in Test 14.

The power supply was terminated in Test 16 shortly after the beginning of this flow reversal, just after the first signs of dryout, which occurred slightly earlier than in the other two tests. Following power switch off, the deceleration in the rate of growth was rather more marked, there being no signs of vapour at either the 1100 or 250 mm levels. Vapour collapse was terminated 2.07 seconds after power shut off, although the integrated void reveals a subsidiary bubble somewhere in the system which persisted for another .68 sec. The location of this bubble is not clear.

Test 22 (Fig.25) was carried out using the same heat flux as tests already described and with the same initial flow, although because of a lower degree of inlet throttling, this was achieved with a smaller pressure drop. Boiling began in this case with a flow velocity about the same as that found in tests 14 and 25, but with a pressure drop at that time of only 0.5 bar.

The first indications of boiling, received from the outlet flowmeter and pressure monitors, were recorded at 9.59 seconds, but the amount of vapour produced was insufficient to give any value for the equivalent void. Between 9.78 and 9.98 seconds, a bubble was produced which was of measurable size - 30 mm equivalent. This bubble seems to have missed the Chen detector at 700 mm, although the coolant thermocouple signal at that level, and the one at 580 mm shortly earlier, can both be interpreted as indicating the presence of vapour at these levels. The bubble plotted in Fig.25 has been given a gradient which corresponds to the inlet flow velocity.

Minor pressure pulses marking collapses of these preliminary bubbles are found before a period of continuous growth which marks the beginning of the main bubble at 9.98 sec. Growth of this boiling region is significantly faster than those hitherto considered if its rate of development is estimated from the time of its nucleation: however if the "zero time" is based on the instant at which the first indications of boiling were received, then the rate of growth over the 1st second is very similar to values observed in Tests 14, 16 and 25, although subsequently, e.g., at 1.5 sec. after nucleation (t_B + 1.5 sec), its growth rate has accelerated. Flow reversal appears rather earlier, at about t_B + 1.44 sec, and dryout too arises more rapidly, at t_B + 1.7 sec. After two partial collapses and secondary growth periods, after power has been turned off, the vapour collapses finally at t_B + 5.35 seconds. No dryouts were detected below the 500 mm level.

Tests 13, 15 and 24 were carried out using approximately the same heat flux 98 - 99 w/cm^2, and the same system pressure. The inlet flow in Test 13 was highly throttled and no superheat was observed, whereas 15 and 24 were practically unthrottled, the

initial pressure drop across the test section and throttle valve being less than 1 bar. Superheats in these latter two cases were 22 and 68 ^{o}C respectively.

Test 13 (Fig. 26) begins with the growth and collapse of two small bubbles: the first of these causes some response to thermocouples at the 580 mm level, but no signals appear on any of the Chen detectors and the exact location of these bubbles is not certain. Following the collapse of these, voiding begins again close to the 580 mm level, without observable superheat. This void grows relatively slowly, at about half the rate of those in the 14/16/25 group of cases when time is zeroed from receipt of the first signal. Progression of the boiling region downward into the channel is relatively slow: 2,5 seconds to reach the 300 mm level, and boiling progresses not far below this point. Power was terminated at 2.62 seconds, which coincided with the first dryout signal, but which followed inlet flow reversal (t_B + 2.31 sec.) The fraction of the boiling region which is filled with vapour is relatively low in this case, typically about 50 to 60 %.

Boiling in Test 15 (Fig. 27) began with the generation of a fairly small and short lived bubble, which nucleated with the release of some 22 ^{o}C superheat. This occurred close to the 580 mm level, at which the superheat was measured, and extended downward, giving a signal on the Chen detectors at the 500 mm level. This downward spread led to an inlet flow reversal within .05 sec. At the collapse of this bubble, a second is generated, somewhat lower in the channel. This produced signals at the 400 and 500 mm levels soon afterwards, and led to an almost instantaneous flow reversal. Power was terminated 0.5 sec after the nucleation of this bubble, following its first partial collapse. The bubble subsequently underwent two further pulsations before finally collapsing at t_B + 1.51 sec. Dryouts were only achieved after power termination.

There are indications of two subsequent bubbles persisting after collapse of the main boiling region: the first of these was recorded on the Chen detectors at 500 mm: the position of the second is not known.

Test 28 involved the rapid and complete cessation of flow, and the records are illustrated in Fig.28. Boiling began within a second of initiation of the transient, apparently with about 27 ^{o}C superheat. The resultant growth of the vapour region was rapid, the lowest Chen detector at 250 mm giving vapour signals within 0.75 sec of nucleation and the highest, at 850 mm, soon after t_B + 1.5 sec. Power was terminated soon after the first dryout signals were received when the upper boiling interface was at about the 1000 mm level, and the lower, close to channel inlet. The termination of power was followed by a series of oscillations of the upper interface, indicated clearly by the two uppermost Chen detectors, initially at a frequency of about 1.5 Hz, but subsequently slowing to about 0.5 Hz as temperatures became more equalized in the upper part of the channel. These oscillations gave a clear signal on the outlet flowmeter, and also on pressure monitors and thermocouple 39 sited at the 1100 mm position. Dryout was extensive throughout the heated region.

3.6 Flow Regimes

There are certain features of the results which give some indication of the flow regimes to be found within the boiling region. It would appear from the Chen detectors that, close to the lower boiling interface, there is a region in which vapour and liquid are mixed as a virtually homogeneous mixture: this may be exemplified by reference to Test 27 (Fig. 24) in which the Chen signals C2 and C3 at the 500 mm level give rapidly fluctuating signals between 13.7 and 14.4 seconds, i.e., from the time at which the boiling interface reaches that level, until it is about 100 mm below it, after which much less liquid entrainment is indicated. Slightly below, at the 250 mm level, a similarly fluctuating signal is found for the first 160 msec or so after vapour is indicated and during which time power is switched off: by the end of this time the boiling interface is again about 100 mm below the Chen. Shortly afterwards the direction of movement of the lower interface is reversed, and from 15.04 to 15.2 sec. considerable liquid entrainment in the vapour is apparent. On the next downward move this is less apparent, but as the in-

terface moves upwards again, between 15.7 and 15.8 sec. an apparently homogeneous mixture is again observed. At this stage, power has been turned off for about 1 sec: subsequently the effect is not observed.

On the upper interface of the boiling region, somewhat similar signals are observed from C4 at 700 mm between 13.5 and 14.4 sec., and at C5, 850 mm, from 14.0 to about 14.4 sec.. After this latter time, continuous vapour is observed for the next couple of seconds or so. The cause of this behaviour is not immediately clear, but is presumably associated with the radial temperature distribution, which leads to earlier voiding of the central subchannels, leaving plentiful supplies of liquid to be swept from the edge channels upwards by vapour flow. Re-entry of liquid from above may also be a contributing factor. That the involvement of the radial temperature profile may be influential in this respect is suggested by the fact that the clearest examples of this form of behaviour are all those in which no detectable superheat was found. Tests in which intermediate values of superheat were found exhibited these two phase regions to a lesser extent, and Test 24, in which the superheat exceeded the radial temperature difference shows a much more marked steplike transformation from vapour to liquid, even after several oscillations.

About a second or so after power termination, a rather different form of flow regime is encountered, initially in the lower part of the boiling region, but which moves upwards in time through the void/time plane. This appears to have the characteristics of plug flow, i.e., plugs of vapour separated by similar, usually rather smaller plugs, of liquid. This may be seen in Fig.24 (Test 27), beginning at 500 mm at about 16.75 sec. and reaching the 850 mm level about 0.5 sec. later. The signals at 500 mm at around 16 sec., which correspond to the upward movement of the lower interface, may be seen in similar light. The same effect appears clearly in the Chen signals from Test 16 (Fig.7), from 15 sec. onward, and to some extent in most of the tests, though not always so clearly: it is not always possible to differentiate the signals from those attributed to homogeneous flow at the lower boiling boundary. This type of flow is clearly

present in the final stages of the high superheat case, Test 24- e.g., C2, 3 and 4 (Fig.15).

The time to dryout of the liquid film is dependent upon the net rate of mass transfer from the clad, and important factors in this are carry up of liquid from the homogeneous mixture below, the down carry of drops from re-entering liquid above, flooding, stripping of the film by vapour flow and the upward passage of liquid slugs, as well as simple evaporation. From the results it is possible to estimate the equivalent thickness of liquid film which would lead to dryout by evaporation in the same time as was measured. These values appear in the Summary Table, and it is clear that in general the effective values of film thickness are greater than the instantaneous values, which are known from previous work [3] to be typically of the order 0.1 mm. The difference can amount to as much as a factor 12, though factors of 8 to 10 are more common, and clearly illustrates the importance of replenishment of the liquid film. The high superheat of Test 24, which led to the most rapid vapour growth away from those zones which eventually dried out, also led to the smallest value of equivalent film thickness - about 0.20 mm. Similarly, Test 15, in which 22 ^{o}C superheat was recorded, also gave rise to a significantly lower value of about 0.31 mm. Simple calculations show that the stored superheat energy in the pin cladding is sufficient to evaporate about 10^{-3} mm of sodium per degree of excess pin temperature. Allowance for this stored energy increases the equivalent film thickness from .20 to .27 mm and from .31 to .33 mm in these two instances. It is, therefore, clear that stored heat in the pin cladding is insufficient to account for the relatively low values found in these two high superheat cases. There will be an additional contribution from the boron nitride insulation and magnesium oxide filling of the heater pins, but the importance of this component is more difficult to assess because of the longer time scale over which it is released. Thermal capacity considerations show that its effect cannot be great. It would, therefore, appear that the low film thicknesses deduced from the higher superheat results are primarily a consequence of differences in the flow processes rather than to stored energy. This view would seem

to be supported by the more typical value (1.03 mm) found in Test 28, where 27 ^{o}C superheat was measured with the inlet valve completely closed. However, the results indicate some statistical element.

Of more relevance to the question of flow regimes is the termination of dryout. This seems to arise in many instances following a rise of the lower boiling interface. The results of Test 24 show this clearly: for instance thermocouple 21, the only pin thermocouple at the 400 mm level, indicates rewetting at a maximum of lower interface position, immediately after the start of a flow reversal, at 12.9 sec. (Fig.13). 100 mm above, rewetting occurs just after the next maximum and beginning of flow reversal, at 13.8 sec. At the 580 mm level, rewetting occurs one second later as the lower interface moves upwards during the final collapse.

Similar features are exhibited in Fig.22 (Test 25), where the 400 mm thermocouple registers three dryout and rewetting cycles, each rewetting following an upward rise, or at least a halt in the downward progression, of the lower boundary. Dryouts at the two instrumented levels above this are also terminated following similar upward movements. Several of the other tests - particularly the later ones in which dryouts were more widespread and longer lasting - show features which are broadly consistent with this pattern.

The general picture which emerges is one in which the boiling region spreads by means of a series of secondary nucleations below the main boiling region, normally with little sign of significant superheat. This rather confused mixture of vapour and liquid moves upwards, and as it does so, the flow pattern changes towards annular flow as the vapour bubbles burst through the liquid slugs, which are continually growing smaller as liquid is left behind on the pin surfaces. It is not clear whether any meaningful distinction can be drawn between homogeneous and small scale plug flow in this transition region, but it is clear that sufficient liquid is available to produce rewetting in this lower part of the channel. Annular flow, possibly with liquid droplets

entrained, is found in the centre regions of the channel, and dryouts here can be sustained. Following power switch off, the energy required to evaporate the liquid films is no longer available, and upward moving liquid slugs retain progressively more and more of their initial volume as they move upwards along the channel until rewetting is complete. The plug flow regime is then dominant. Although there is no direct evidence, it seems likely that major growth phases of secondary bubbles below the main boiling region take place in the early stages of expansions of the equivalent void. The consequent liquid plug between the two vapour regions is thereby accelerated upwards and gives rise to the rewettings such as are observed at 12.8 and 13.8 sec. in Fig.13 (Test 24). This seems a little surprising, since pressure in the system is greatest when the bubble size is at an oscillatory minimum; one might expect such subsidiary nucleations with the system at its lowest pressure. It could, therefore, be deduced that secondary nucleation takes place at about the time of the preceding void maximum, but this bubble fails to grow rapidly because of the increasing pressure during void contraction. The boundaries of such a bubble would, therefore, lie as two lines close to and parallel with the original boiling boundary, but which separate and widen as soon as pressure begins to fall, i.e., on the next void expansion.

3.7 Analysis of Dynamic Pressure and Acoustic Signals

In Test 25, inlet flow reversal followed by dryout occurred after 2.1 sec of boiling (Fig.22). At the time of flow reversal, the boiling region extended over about 0.8 m. The dynamic pressure and acoustic signals recorded during this period (11.5 to 13.5 sec) were subjected to a detailed analysis. Fig.29 shows the boiling auto-power spectral density for the three transducers A_1, S_2 and P_4 and the related background spectra measured immediately before the onset of boiling. Although all three transducers are at the same axial position, agreement can be found only within the range up to about 100 Hz. The signal power of the Kaman transducer S_2 drops very quickly to the background while the piezoelectric microphone A_1 shows a nearly uniform signal rise up

to two kHz. Only the piezoelectric quartz pressure transducer P_4 exhibits some frequency peaks while the signal power also decreases to the background value at about 2 kHz. Comparison of the three pairs of plots shows that the identification of the real spectrum of boiling noise is extremely difficult. The coupling section between the liquid and the sensor causes variation and attenuation of the spectrum to such a degree that only a comparative evaluation with the undisturbed background from the same sensor seems to be useful.

Another important problem is the axial transmission of dynamic pressure and acoustic signals. Fig.30 shows for the same run a comparison with the background of auto-power spectral density of the four Kistler quartz pressure transducers. The power densities of P_4 and P_5 are increased during boiling by approximately one order of magnitude while the spectral distribution remains nearly unchanged. A conspicuous phenomenon is the decrease of the spectrum down to the value of the background beyond 2 kHz.

Fig.31 is a plot of the auto-power spectral density of acoustic measuring points A_1, A_2 and S_5 for the same experiment. At the latter measuring point which consisted of a solid coupling bar, penetrating into the sodium pool, and a piezoelectric microphone, resonances occur in the background spectrum at 16.6 and 19.0 kHz. They are attributed to higher order half wavelength excitations of the waveguide. They depend on the geometry and are very distinct in the present case within the range above 16 kHz. The experimental results show that both the acoustic background and the acoustic spectrum obtained during boiling have bandwidths of at least 20 kHz, since the higher frequencies could not be recorded. The frequencies recorded up to 20 kHz are probably responses of the structure, which are caused by the excitation of the system characterized by a complex transmission function.

The comparison of signal-noise ratios for the different axial measuring positions in Figs.30 and 31 shows that the rise in the signal power due to boiling is a maximum in the boiling zone proper (P_4, P_5, A_1, A_2). Both downwards (P_3) and upwards towards the sodium pool (P_6, S_5) a marked decrease of the signal-noise ratio

can be observed for both tranducer types. It seems possible that this poor axial transmission behaviour is a fundamental property of the 7-pin bundle with its small cross section as compared to the fuel element.

3.8 Comparison with Single Channel Experiments [4]

In Fig.32, data obtained from Test 16/14 in an annular test section are plotted together with data from Test 7-2/24. As can be seen from the Table reproduced in the Figure, there are some differences in the starting conditions; in particular flow velocities at the onset of boiling are in the former case 1.1 m/sec, and only 0.33 m/sec in the latter. If the first two small bubbles generated from minor localized superheat and which collapse completely are not taken into account, the inlet velocities for the two tests correspond much better, the value of 1.1 m/sec being reduced to 0.5 m/sec. The axial temperature profile before the onset of boiling is comparable for the two runs considered.

The void develops faster in the case of the annular geometry test, as a result of the greater thermal capacity of the test section - i.e., larger amount of stored superheat energy. Also the frequency and amplitude of oscillation are higher as a result of the different hydraulic characteristics and driving forces; only 34 ^{o}C superheat occurred in the annular test, compared with 68 ^{o}C in the seven pin bundle, and the hydraulic diameters of the channels were 4 and 4.25 mm respectively: likewise the channels were of different lengths. However, in qualitative terms at least, the course of events during the development of the void is comparable for the two tests.

Because of their smaller thickness, heater pin response to changes in cooling conditions are much more rapid in the seven pin bundle. One large bubble is sufficient to decrease indicated pin temperatures at the end of the heated section by about 60 ^{o}C, down to saturation temperature. In the annular geometry, the comparable temperature (T_i in Fig.32) shows only a minor reaction. In spite of its lower thermal capacity, dryout is indicated for the 7 pin bundle only 0.5 sec. after the onset of boiling, where-

as in the annular test section this is delayed until a second after the first ejection. This is probably partially due to the greater superheat in the bundle experiment, but the different geometric distribution of the liquid relative to the heated surfaces could perhaps be of greater importance. Also the more vigorous liquid oscillations in the annular channel, with higher reentry velocities, means that droplets of liquid can penetrate more deeply into the test section, improving rewetting and thereby the cooling conditions.

Inlet flow reversal was observed only 10 msec after the onset of the first ejection in both cases.

4. CONCLUDING REMARKS

A series of ten experiments has been performed utilising an electrically heated seven pin bundle in simulations of the flow rundown/trip failure accident in a fast reactor. The results give valuable qualitative insight into the pattern of boiling development which would occur under these conditions in a real reactor.

Because of loop and heater pin limitations, it was not possible to model reactor conditions exactly. For instance, the length of the heated section, the pressure drop across the channel, and channel outlet pressure all differed significantly from typical reactor values. The effects of these differences were minimised as much as possible by the appropriate choice of inlet conditions. Certain features of the test section, in particular the high thermal capacity of the wrapper and the marked temperature distribution across the bundle, are also unlikely to be found in a real fuel bundle.

Thus, although heater pin pitch and diameter corresponded to those of the SNR fuel element, and the rundown characteristics of the SNR circulator pumps were modelled, considerable care should be taken before applying these results to SNR, or to any other reactor. The results do however provide a valuable source of measured data against which the predictions of computer codes

such as BLOW3 [5] can be compared, and, hopefully, against which the codes can be validated. Once validated, such codes may then be used with greater confidence to predict the course of boiling under reactor conditions.

The results give insight into the types of flow regime which are to be found in the experimental system, and indicate clearly the importance of clad rewetting, which delays the onset of dryout beyond the times suggested by simple models with no rewetting representation. Nevertheless, dryout did occur in all tests, typically within a couple of seconds, and in one case only some 0.57 sec after nucleation. Dryout is believed, however, [6] to be dependent upon channel geometry, and it is not clear how relevant these times would be to reactor conditions. Inlet flow reversal was also found to occur at some stage in every test.

Comparison with the results of single channel annular geometry tests reveals that under similar thermal-hydraulic and superheat conditions, the boiling behaviour is similar too, although differences in the initial radial growth phase arise, because of the different temperature distributions across the channel. Once saturation temperatures are attained in the wall subchannels of the bundle, the boiling phenomena broadly correspond to those in a single channel.

5. REFERENCES

[1] Fröhlich, R., et al.: Analyse schwerer hypothetischer Störfälle für den SNR 300 Mark IA Reaktorkern. KFK 2310, June 1976

[2] Chen, J.C.,et al.: Probe for Detection of Voids in Liquid Metals. Rev. Sci. Insts. 39, pp.1710-1713 (1968)

[3] Spiller, K.H., Perschke, D., Grass, G.: Messungen der Restfilmstärke bei der Einzelblasenejektion von flüssigem Natrium in einem Rohr. ATKE 14-21 (1969) 113-117

[4] Kaiser, A., Peppler, W.: Sodium Boiling Experiments in an Annular Test Section under Flow Rundown Conditions. KFK 2389 (to be published)

[5] Wirtz, P.: Ein Beitrag zur theoretischen Beschreibung des Siedens unter Störfallbedingungen in natriumgekühlten schnellen Reaktoren. KFK 1858 (1973)

[6] Kaiser, A., Peppler, W., Vöröss, L.: Type of Flow, Pressure Drop, and Critical Heat Flux of a Two-Phase Sodium Flow. Nucl.Eng. & Design 30 (1974) 305-315

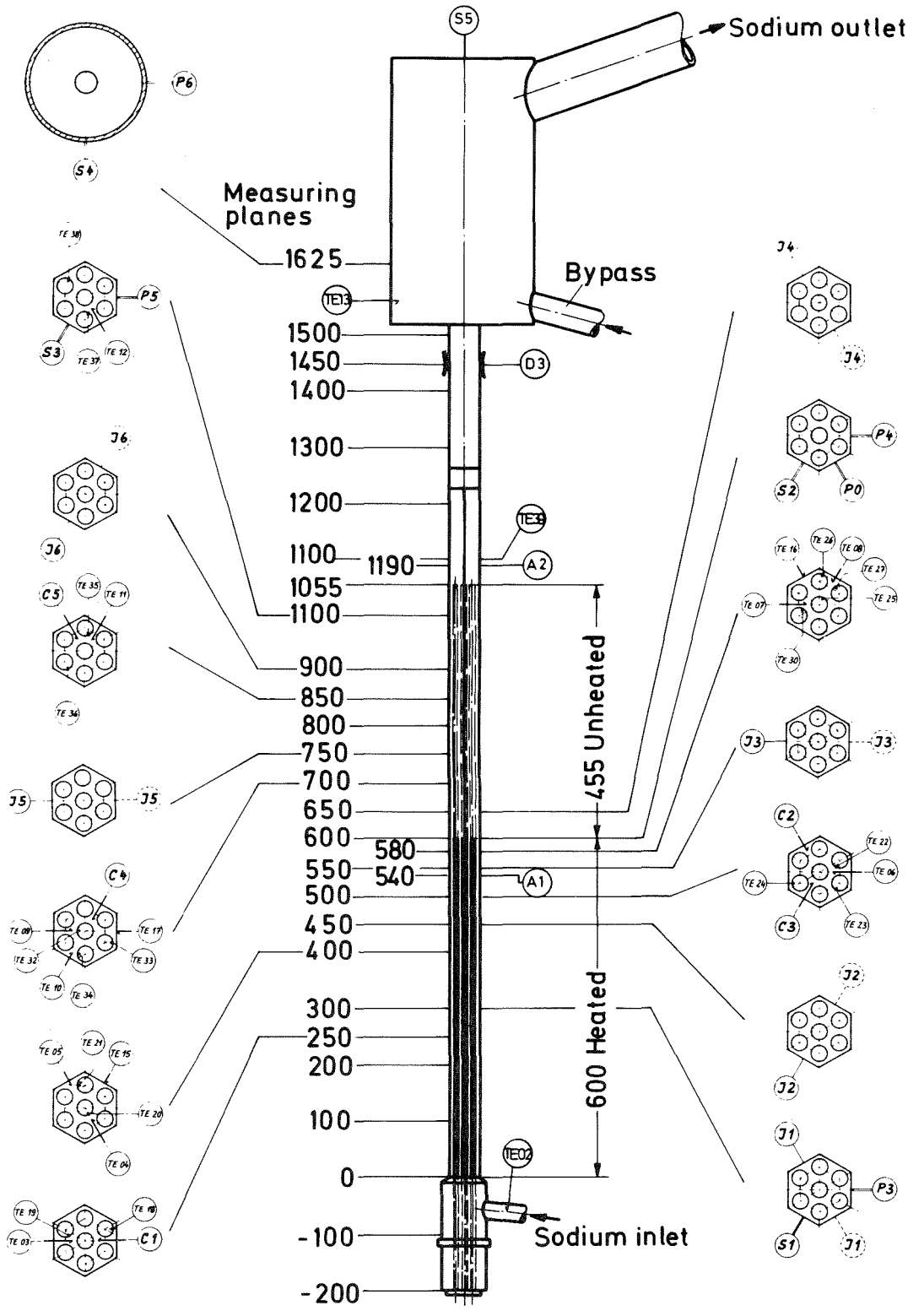

GfK IRE	7-Pin Bundle No 2 Measuring Planes	Fig. 1

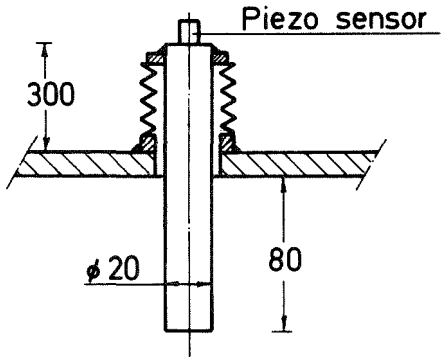

Solid bar waveguide (S5)

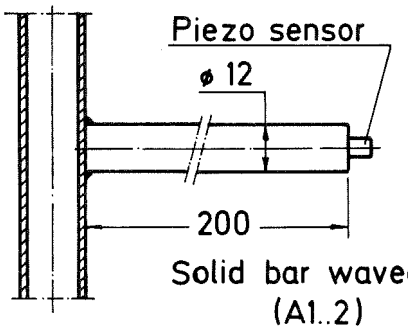

Solid bar waveguide
(A1..2)

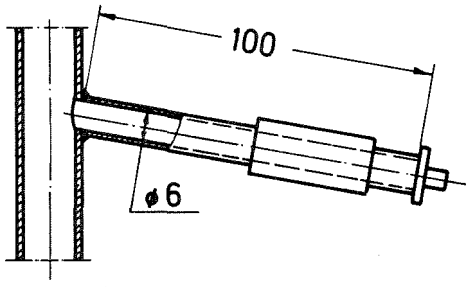

Piezo quartz transducer
(P3..6)

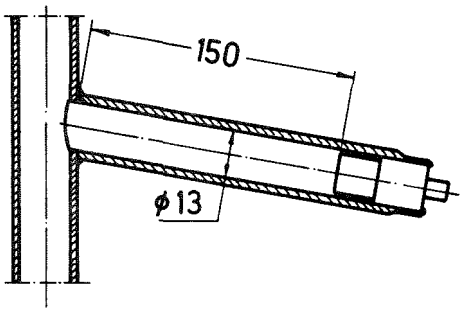

Inductive pressure transducer
(S1..4)

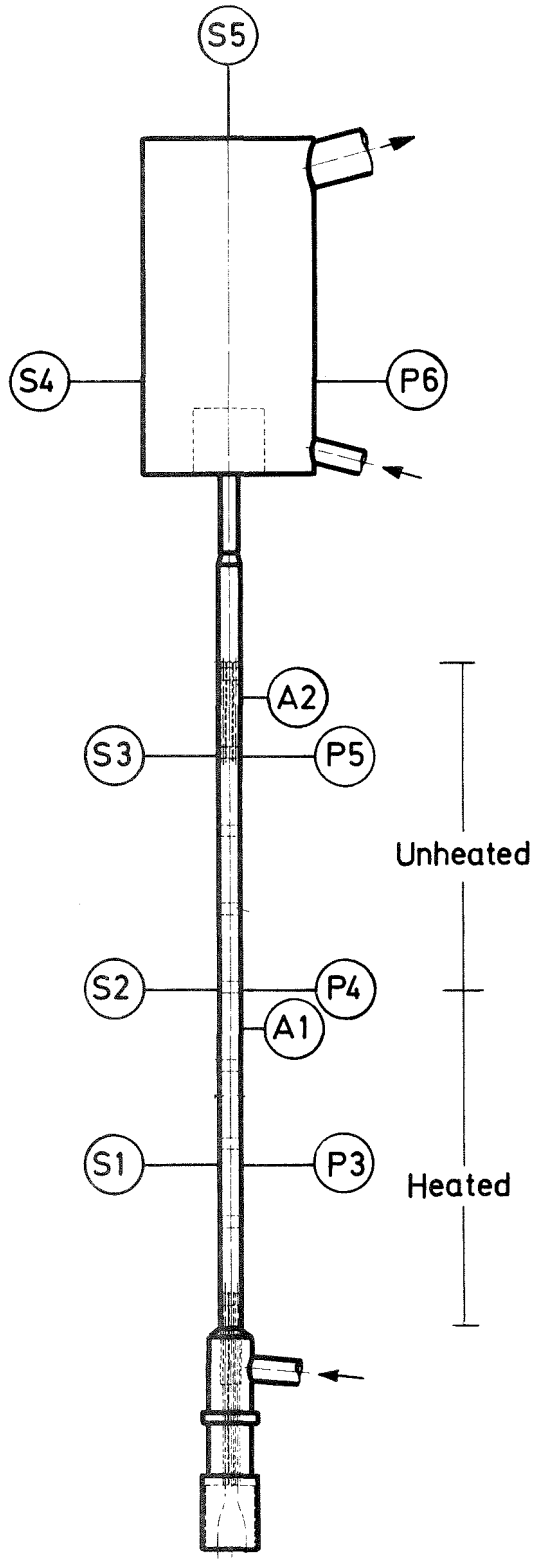

GfK IRE	7-Pin Bundle No.2 Dynamic Pressure and Acoustic Instrumentation	Fig. 2

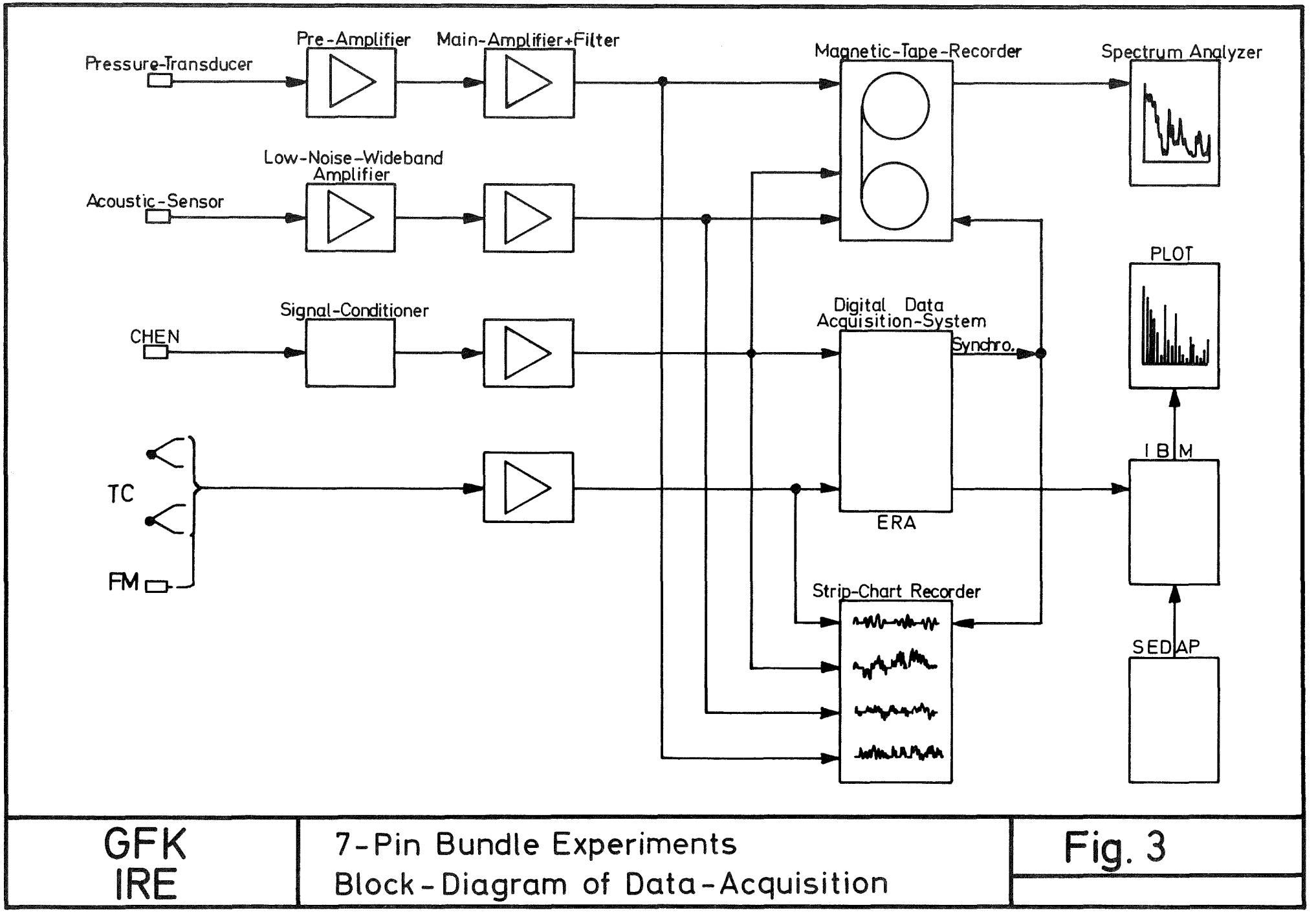

GFK IRE	7-Pin Bundle Experiments Block-Diagram of Data-Acquisition	Fig. 3

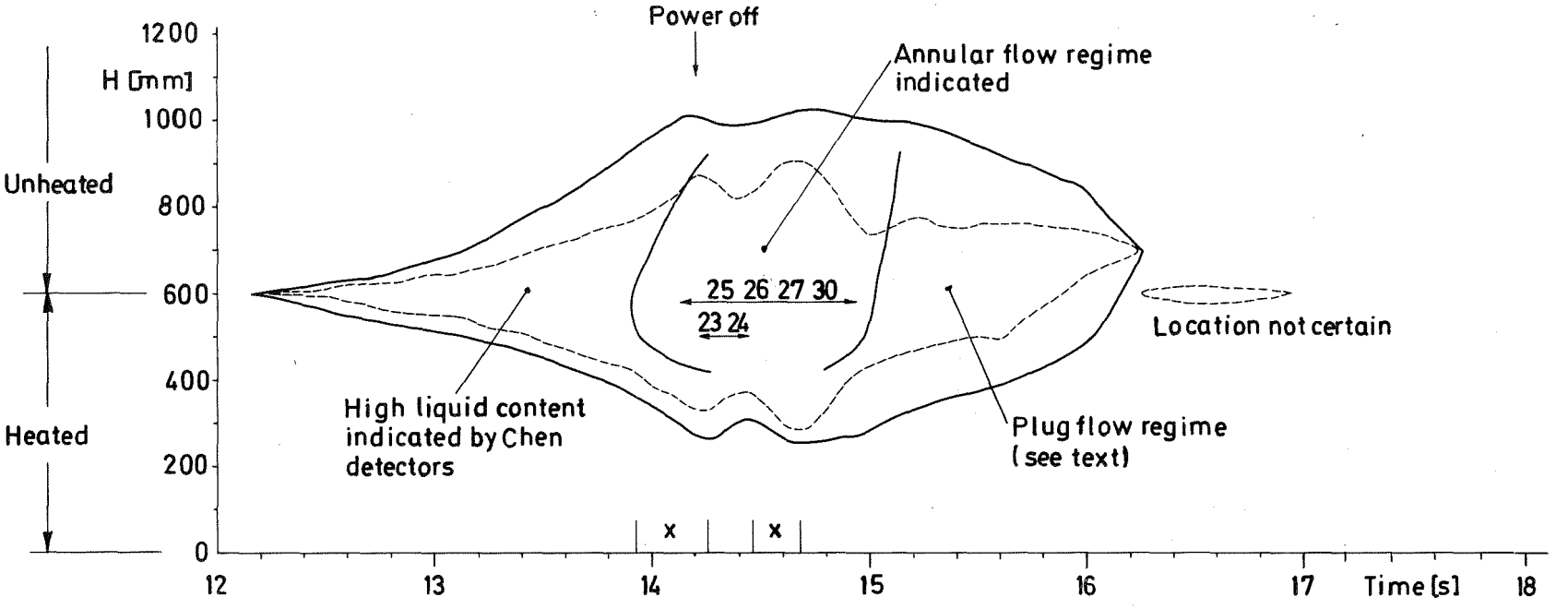

x = Inlet flow reversal
◄——► = Dryout (Numbers refer to thermocouples see Table 1)
——— = Boiling region
– – – = Equivalent void

GfK IRE	7-Pin Bundle, Pump Run Down, Development of Boiling Region and Equivalent Void in Test 7-2/16	Fig. 4

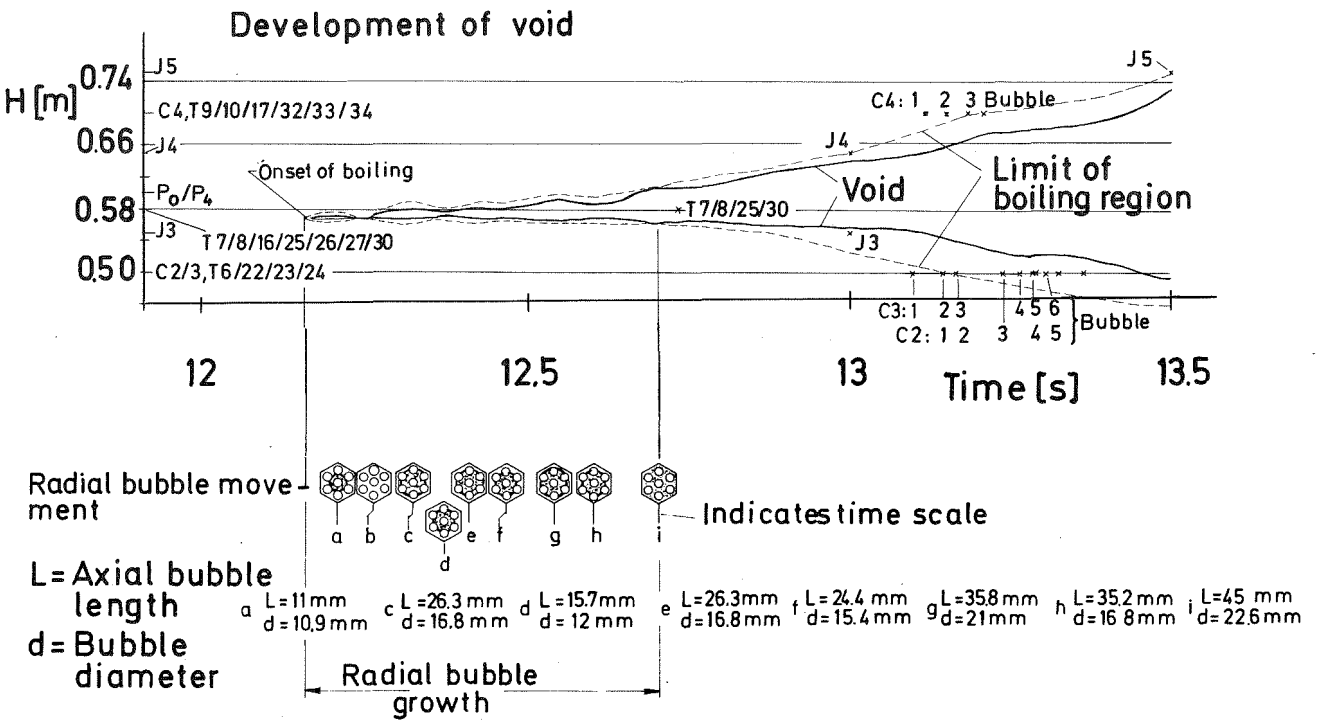

GfK IRE	7-Pin Bundle, Pump Run Down, Early Stages of Boiling in Test 7-2/16	Fig. 5

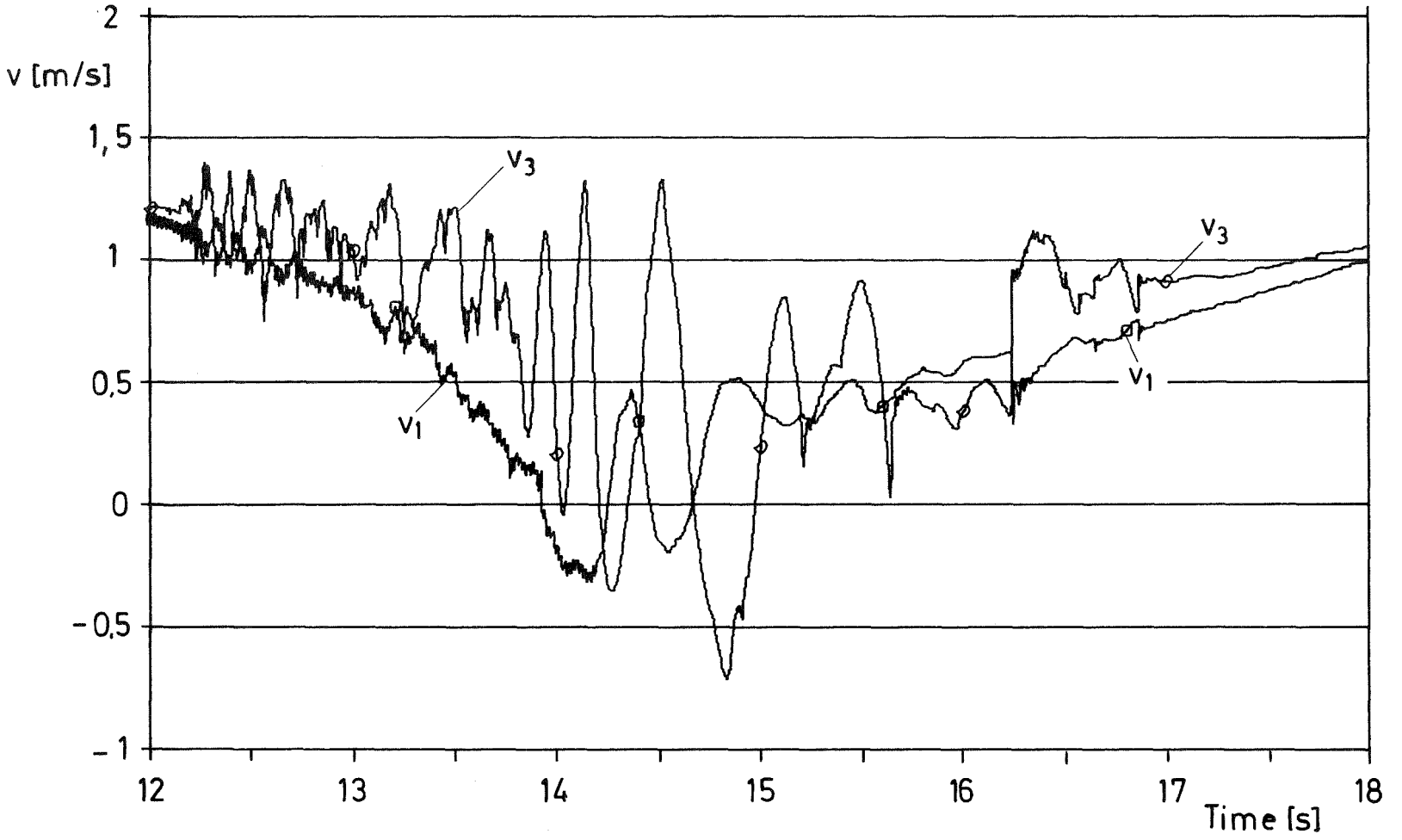

GfK IRE	7-Pin Bundle, Pump Run Down, Inlet (v_1) and Outlet (v_3) Flow Velocities in Test 7-2/16	Fig.6

C5 = 850mm
C4 = 700 "
C3 } = 500 "
C2 }
C1 = 250 "

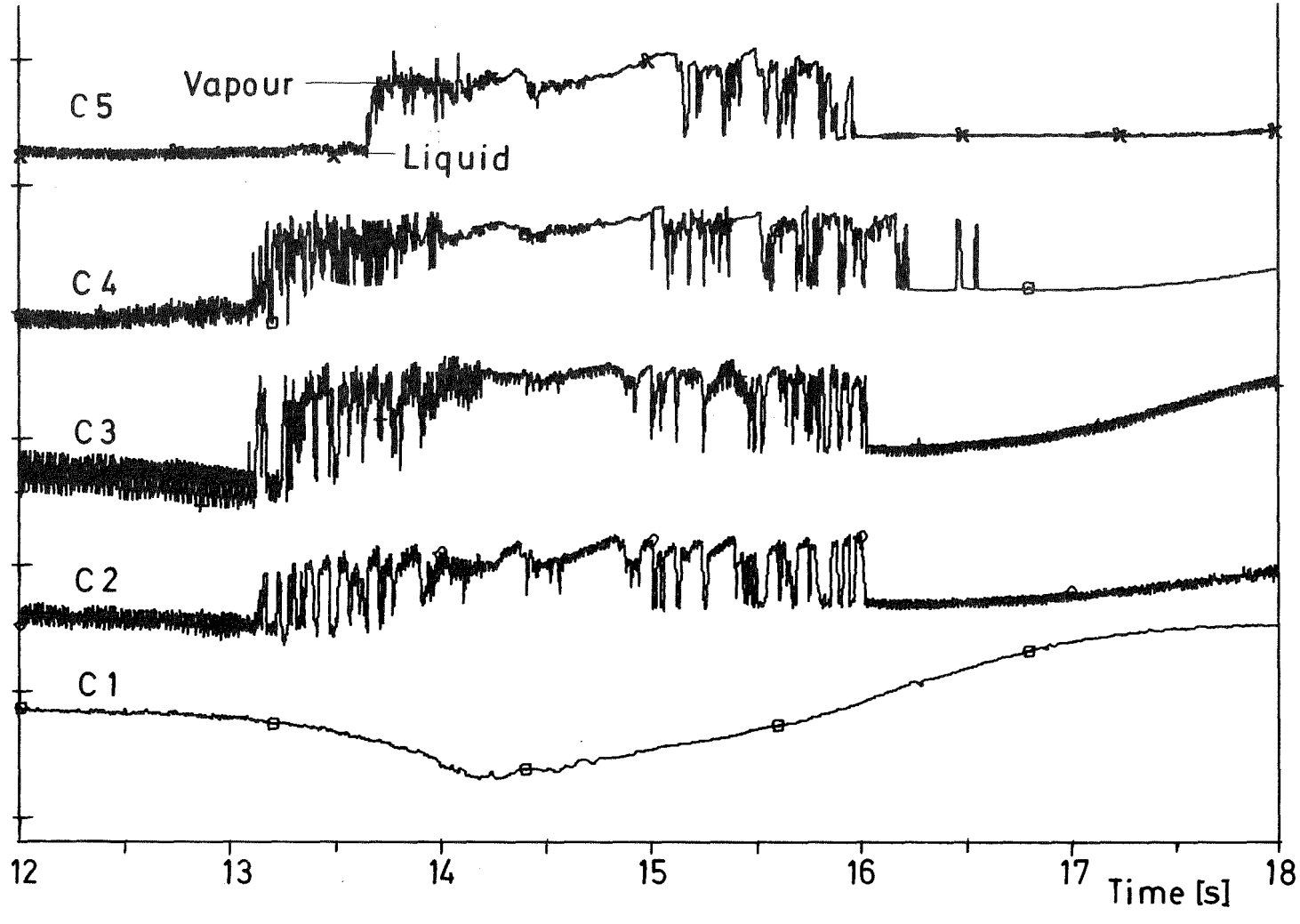

GfK IRE	7-Pin Bundle, Pump Run Down, Chen Signals Received in Test 7-2/16	Fig. 7

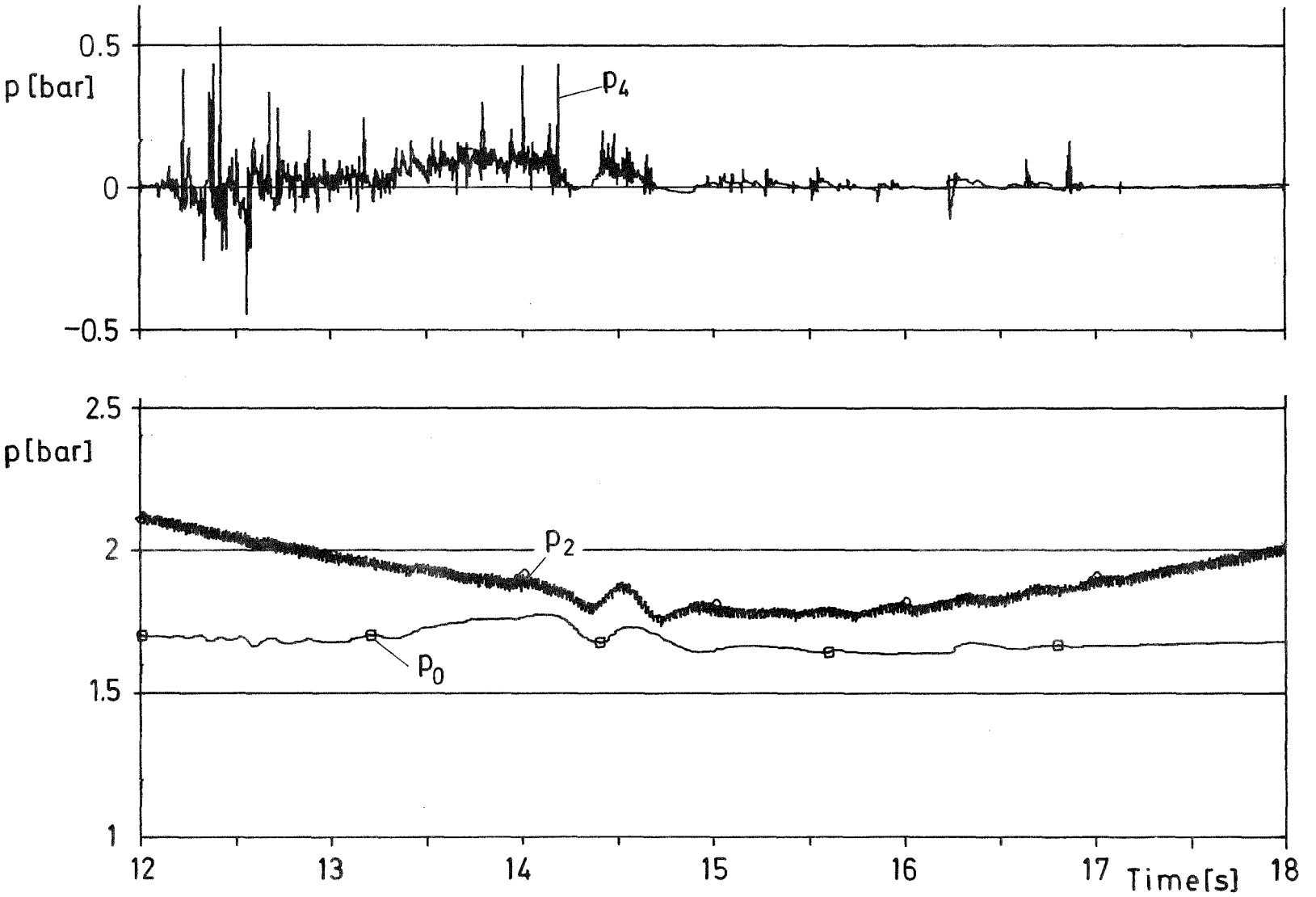

GfK IRE	7-Pin Bundle, Pump Run Down, Dynamic (p_4) and Static Pressures at Inlet (p_2) and Top of Heated Section (p_0) in Test 7-2/16	Fig. 8

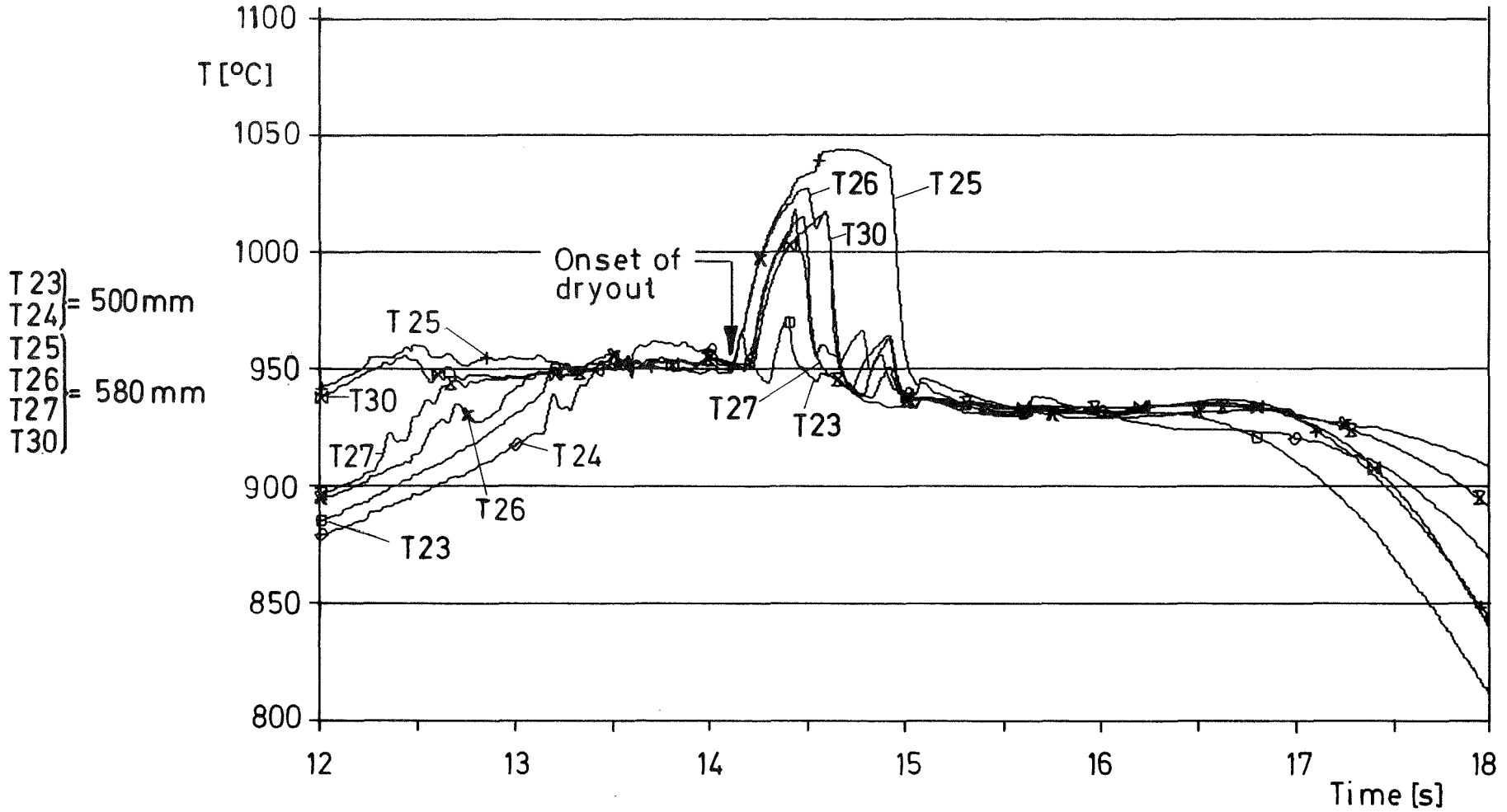

GfK IRE	7-Pin Bundle, Pump Run Down, Sample Pin Temperatures Showing Dryout Signals Monitored in Test 7-2/16	Fig. 9

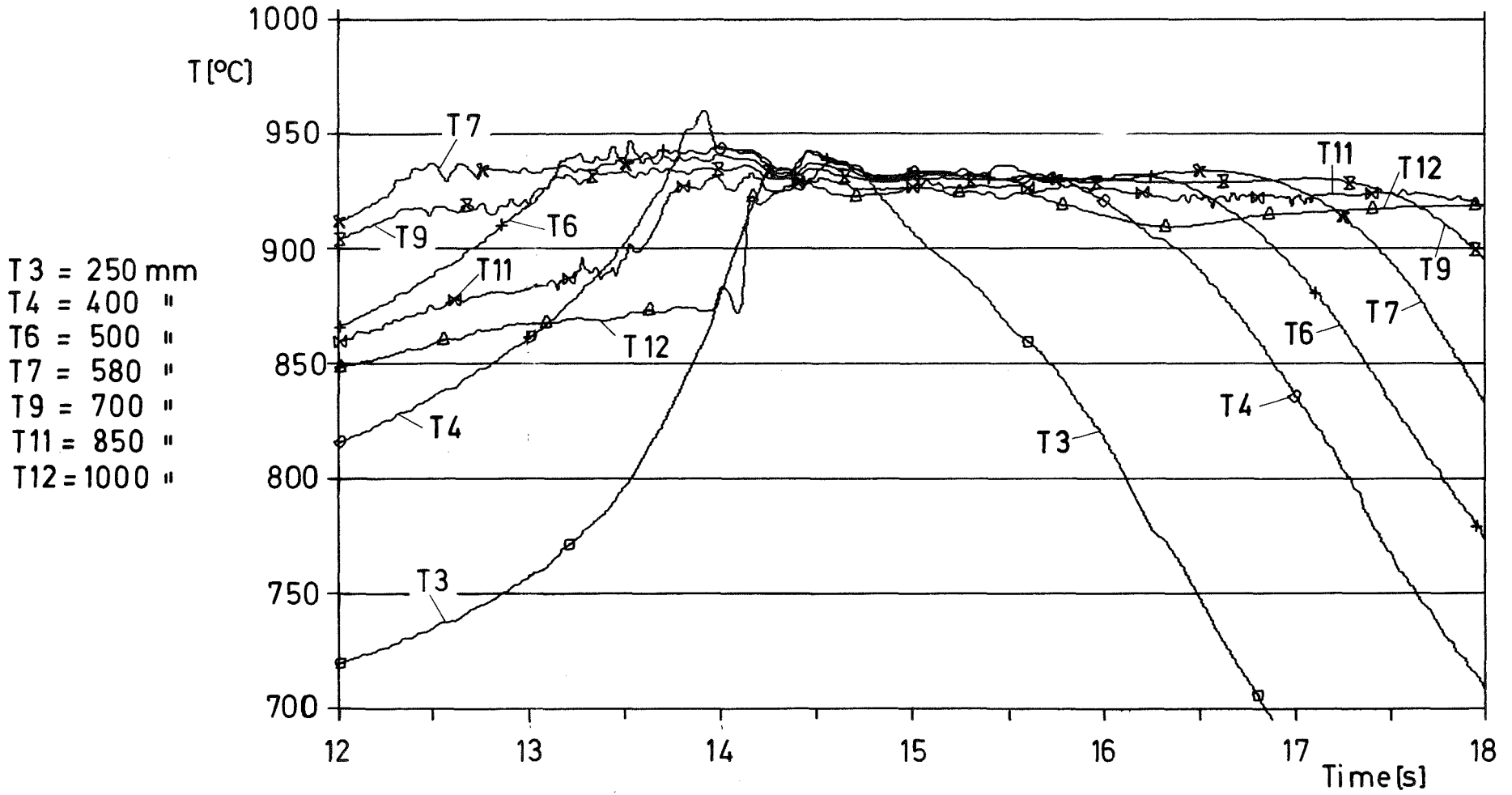

GfK IRE	7-Pin Bundle, Pump Run Down, Coolant Temperatures (Central Subchannels) Monitored in Test 7-2/16	Fig. 10

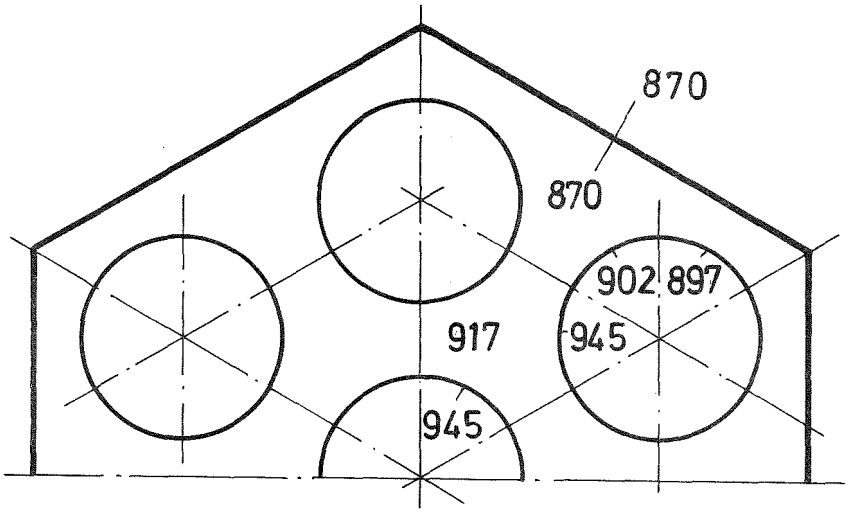

Nucleation
t = 12.15 s
ΔT = 75 °C
T_S = 934 °C

Δ T = Temp.-difference between wrapper and central pin surface

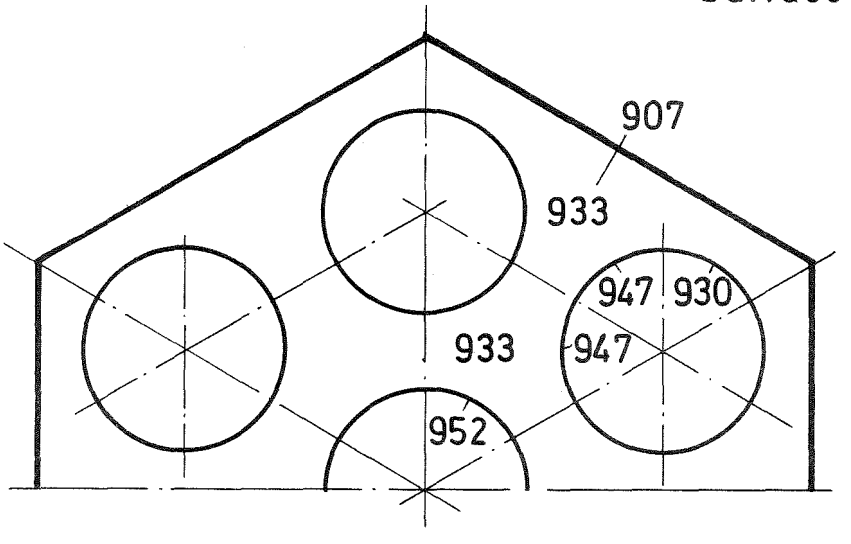

t = 12.7 s
ΔT = 45 °C

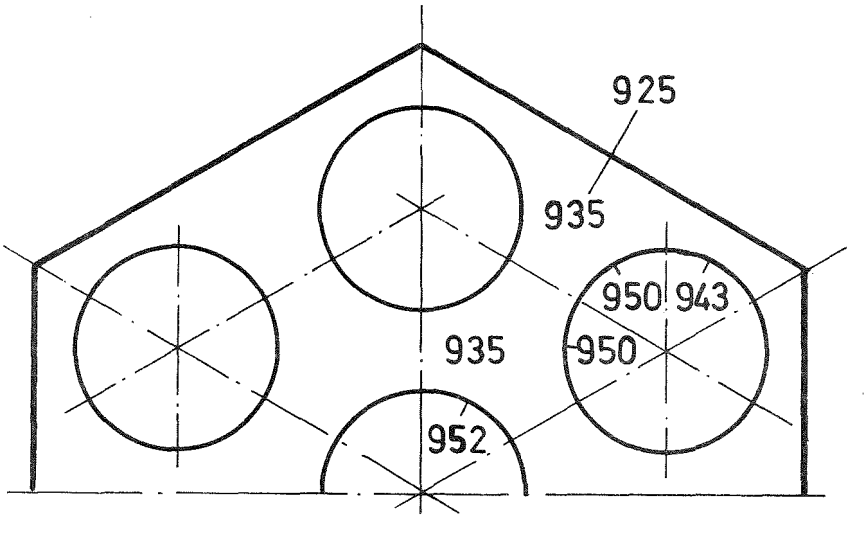

t = 13.1 s
ΔT = 17 °C

GfK IRE	Radial Temperature Profile in Cross-Section 580, Run 7-2/16	Fig. 11

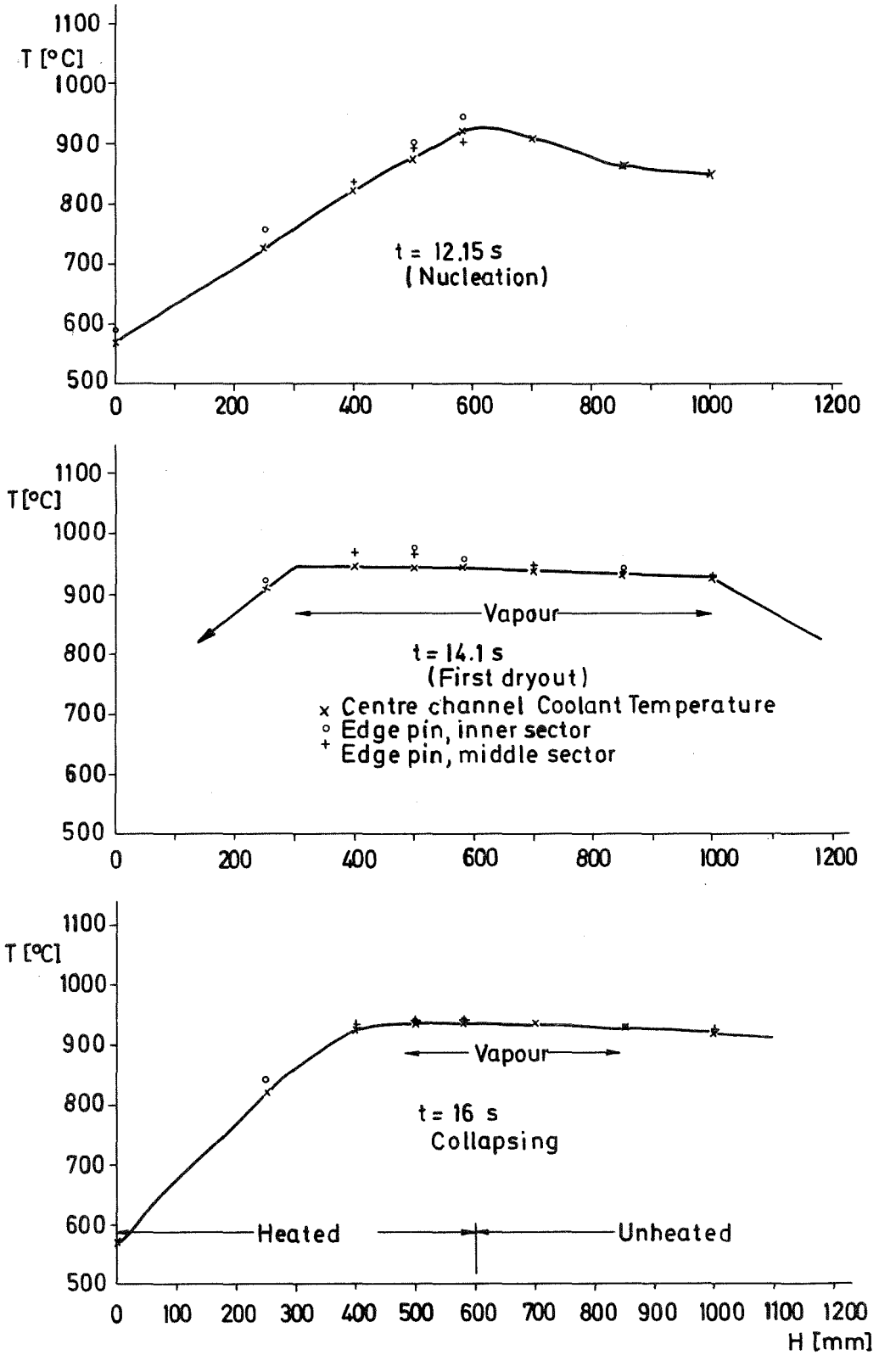

GfK IRE	7-Pin Bundle, Pump Run Down, Test 7-2/16, Axial Temperature Distribution during Boiling	Fig.12

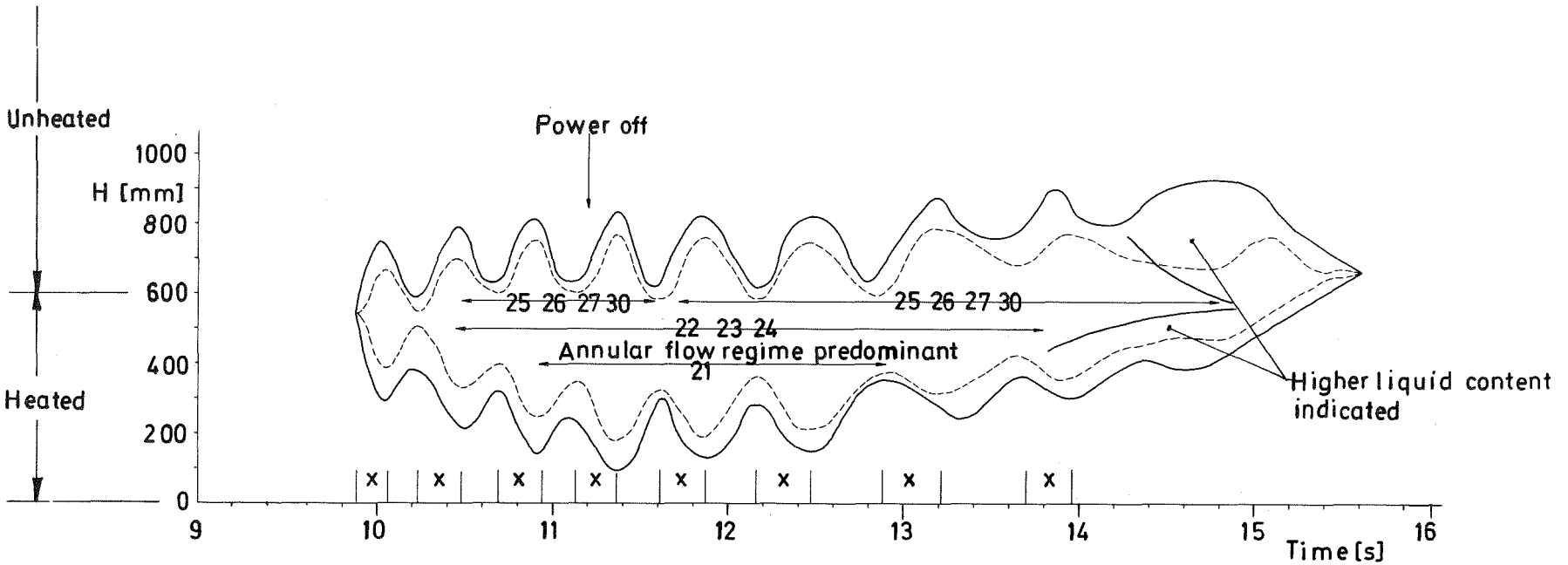

x = Inlet flow reversal

⟷ = Dryout (Numbers refer to thermocouples see Table 1)

——— = Boiling region

– – – = Equivalent void

GfK IRE	7-Pin Bundle, Pump Run Down, Development of Boiling Region and Equivalent Void in Test 7-2/24	Fig. 13

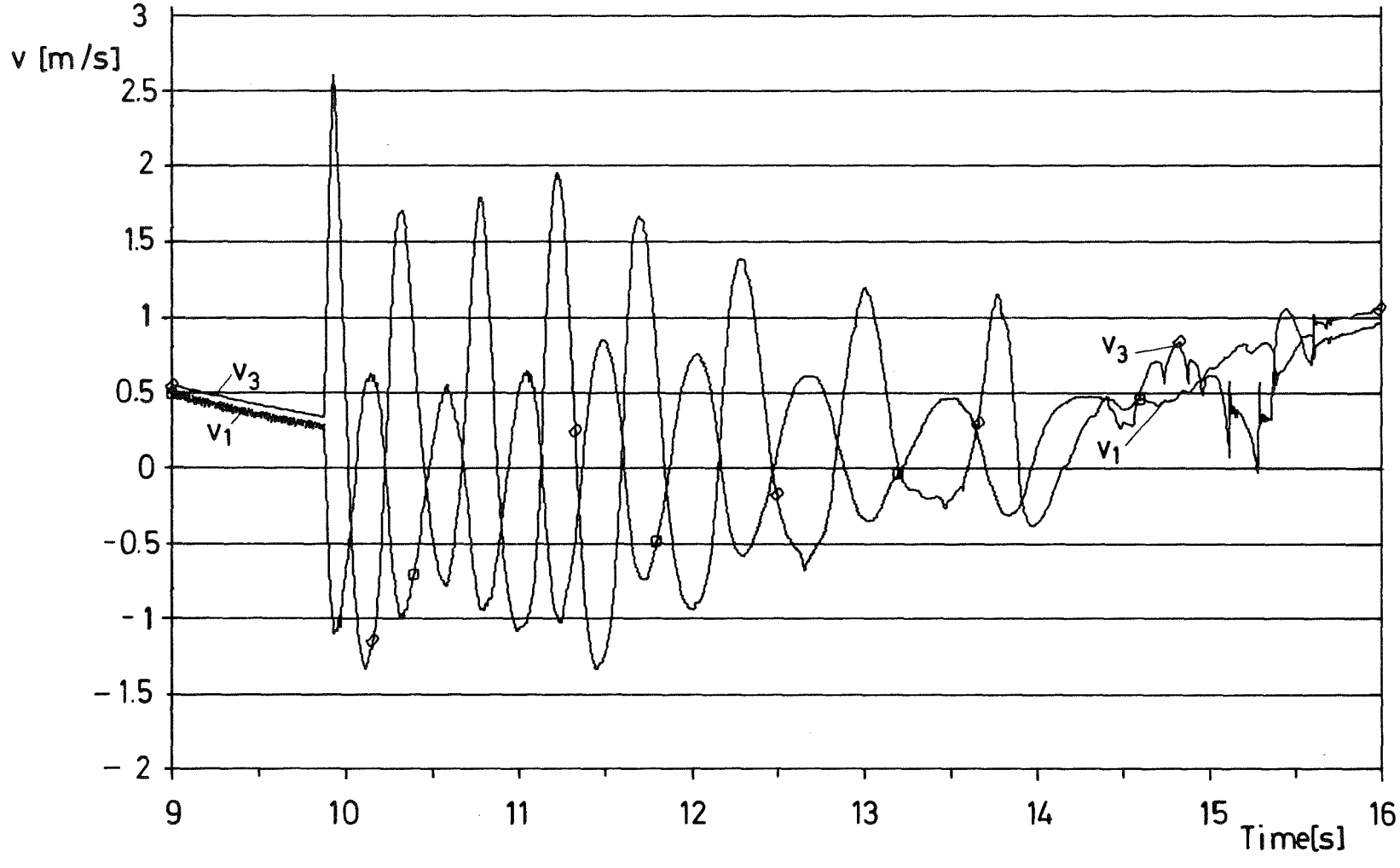

GfK IRE	7-Pin Bundle, Pump Run Down, Inlet (v_1) and Outlet (v_3) Flow Velocities in Test 7-2/24	Fig. 14

C5 = 850 mm
C4 = 700 "
C3, C2 = 500 "
C1 = 250 "

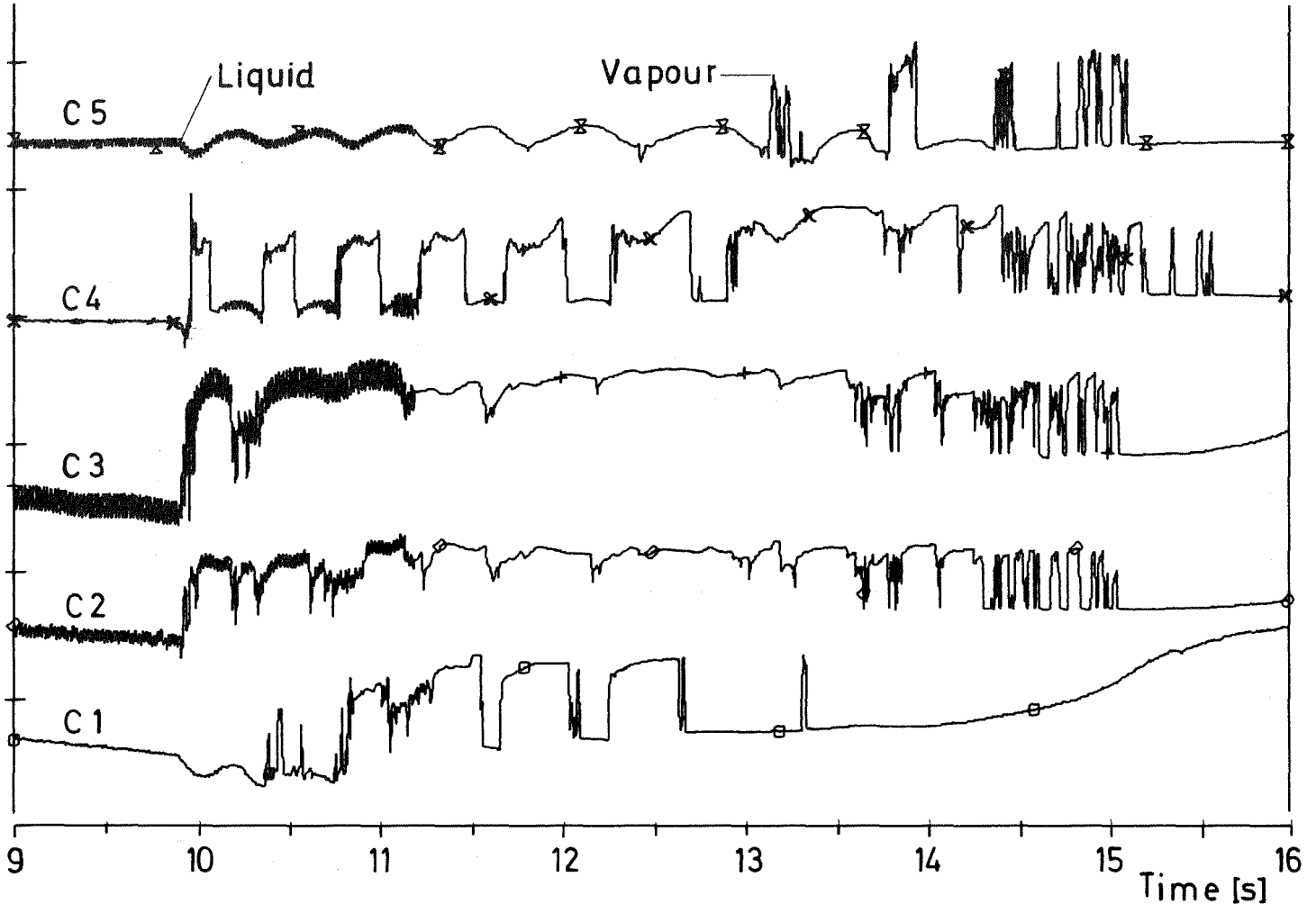

GfK IRE	7-Pin Bundle, Pump Run Down, Chen Signals Received in Test 7-2/24	Fig. 15

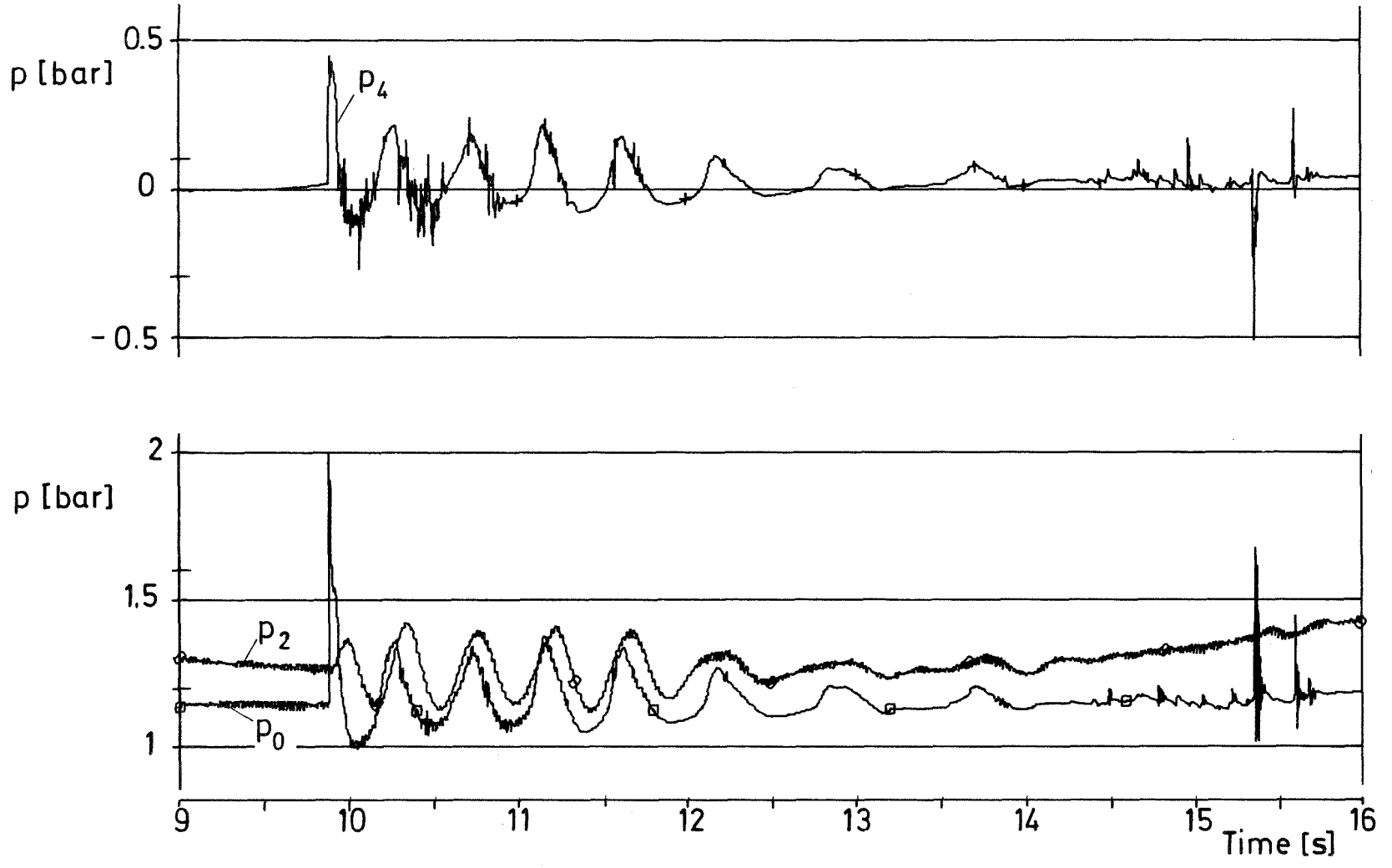

GfK IRE	7-Pin Bundle, Pump Run Down, Dynamic (p_4) and Static Pressures at Inlet (p_2) and Top of Heated Section (p_0) in Test 7-2/24	Fig. 16

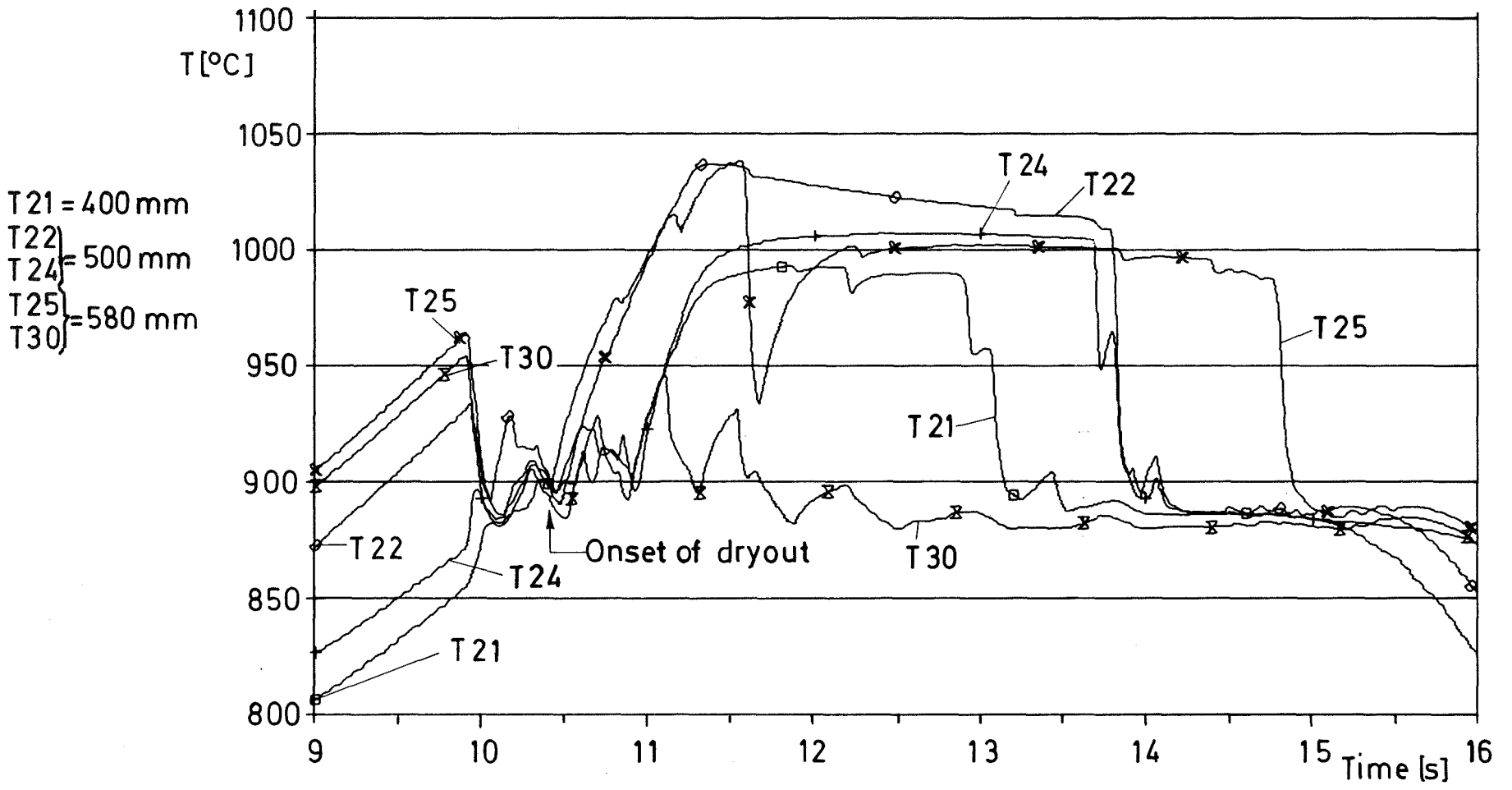

GfK IRE	7-Pin Bundle, Pump Run Down, Sample Pin Temperatures Showing Dryout Signals Monitored in Test 7-2/24	Fig. 17

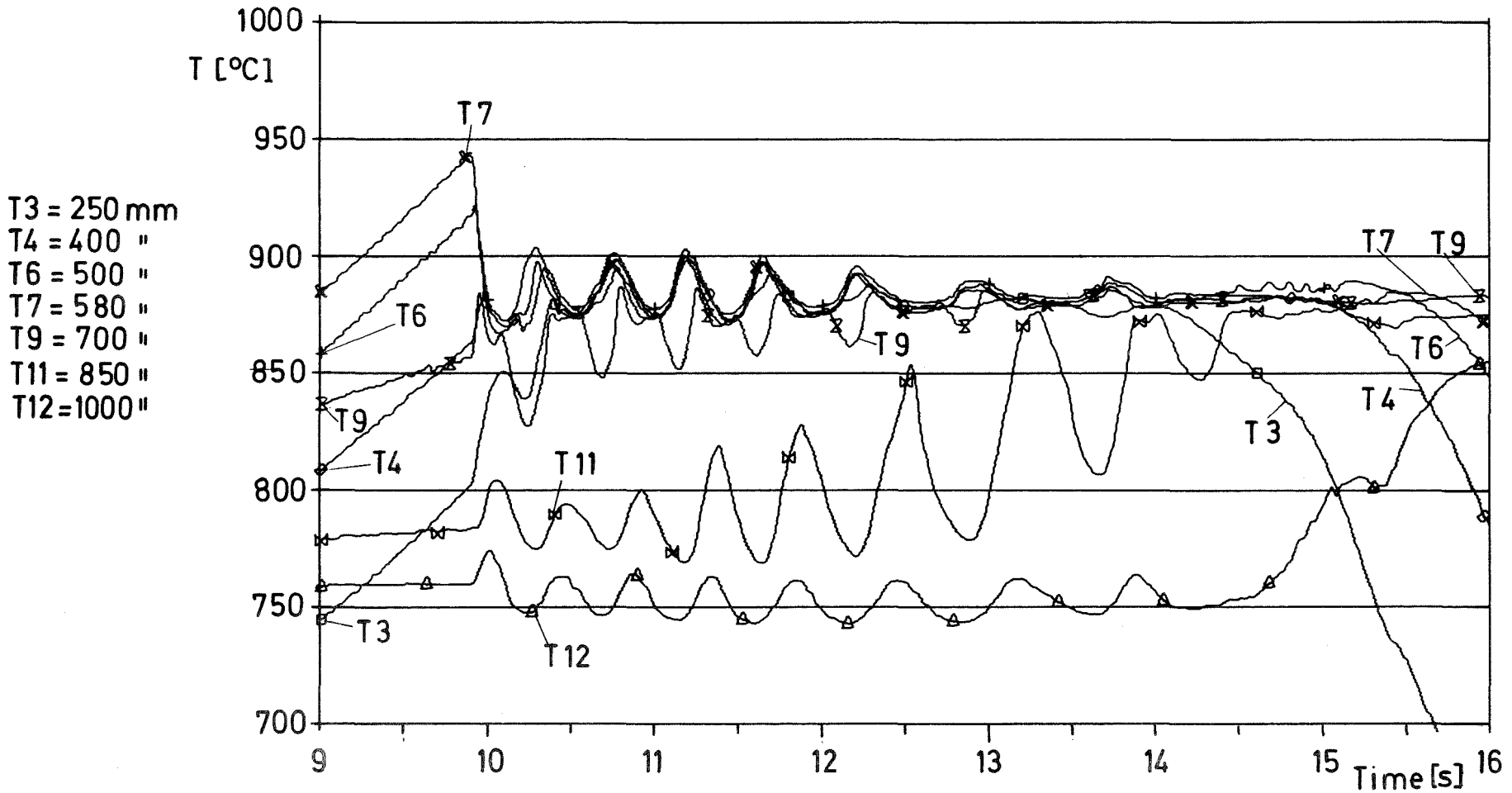

GfK IRE	7-Pin Bundle, Pump Run Down, Coolant Temperatures (Central Subchannels) Monitored in Test 7-2/24	Fig. 18

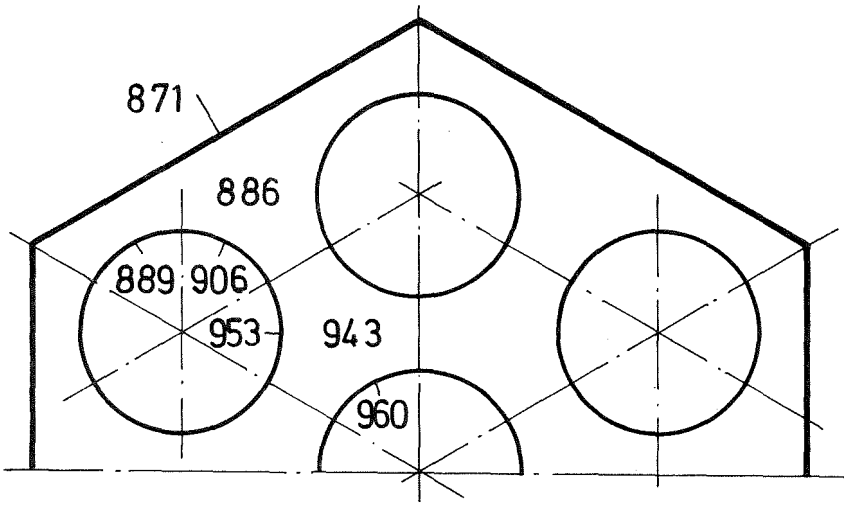

Nucleation

t = 9.88 s

ΔT = 89 °C

T_S = 895 °C

ΔT = Temp.-difference between wrapper and central pin surface

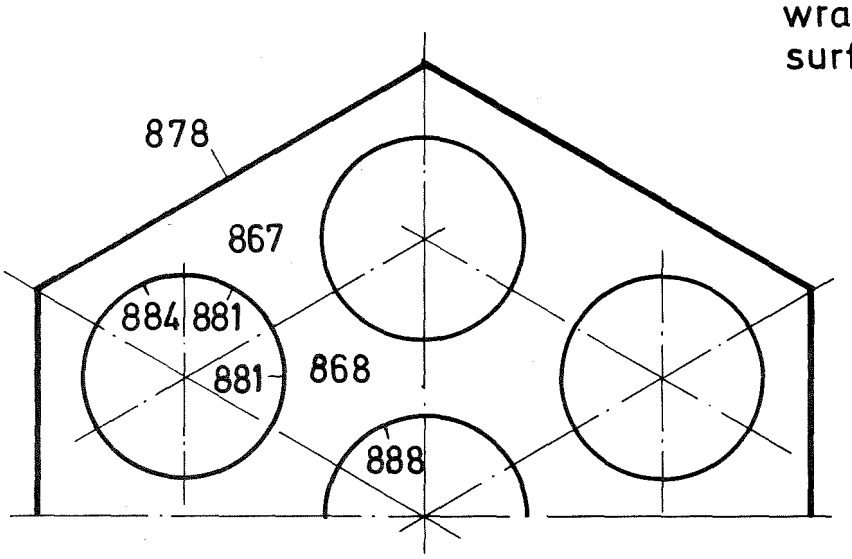

Following first expulsion maximum

t = 10.1 s

ΔT = 10 °C

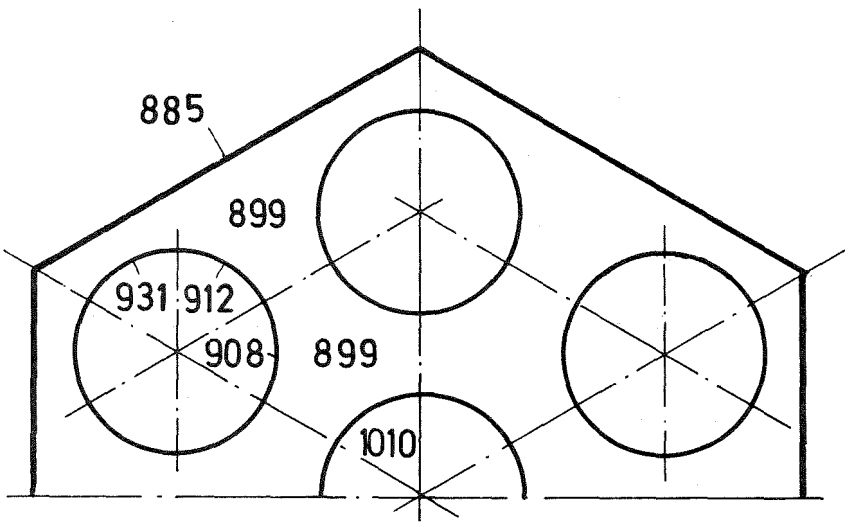

Power switched off (dryout)

t = 11.2 s

GfK IRE	Radial Temperature Profile in Cross-Section 580, Run 7-2 / 24	Fig. 19

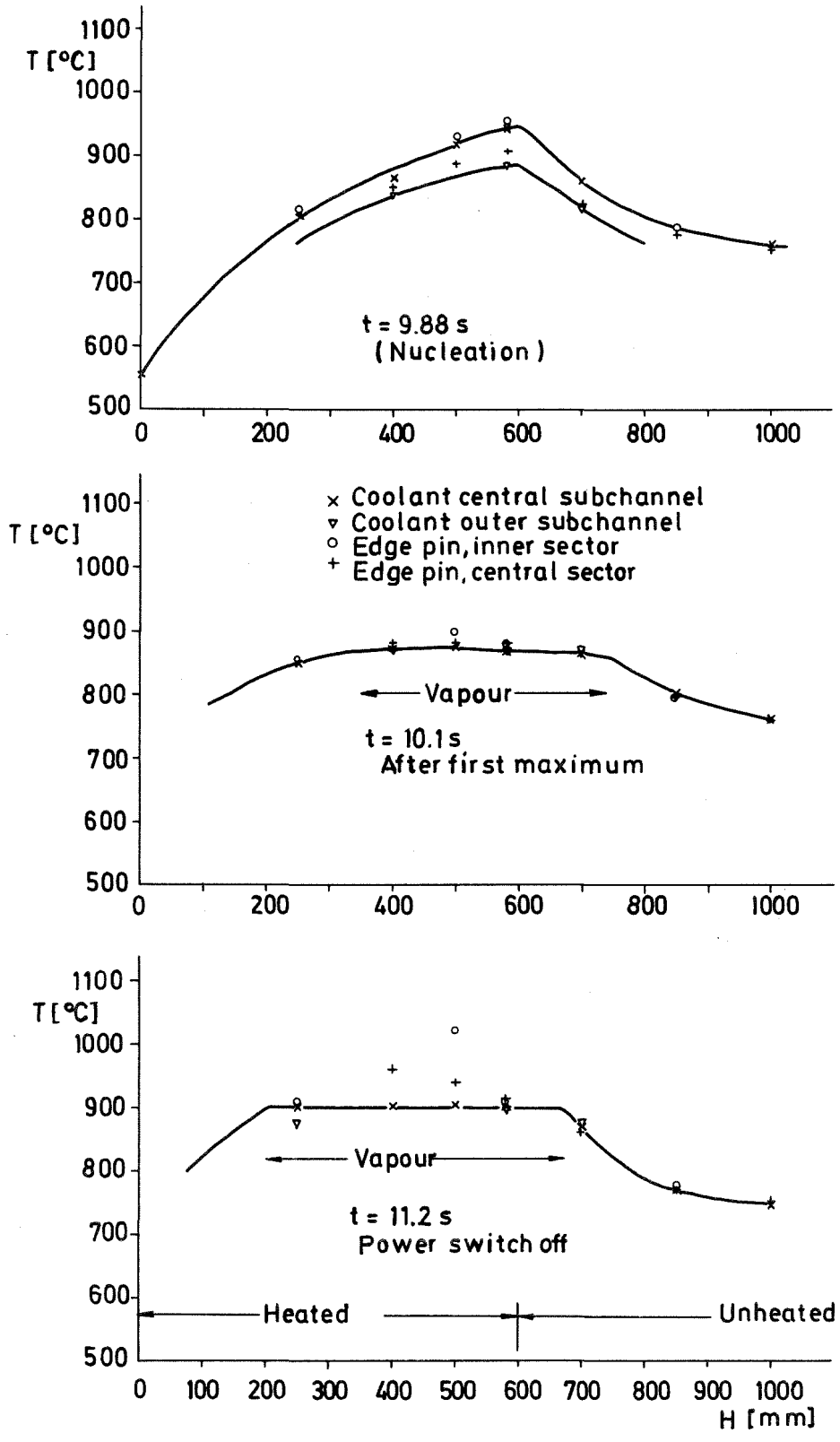

GfK IRE	7-Pin Bundle, Pump Run Down, Test 7-2/24, Axial Temperature Distribution during Boiling	Fig. 20

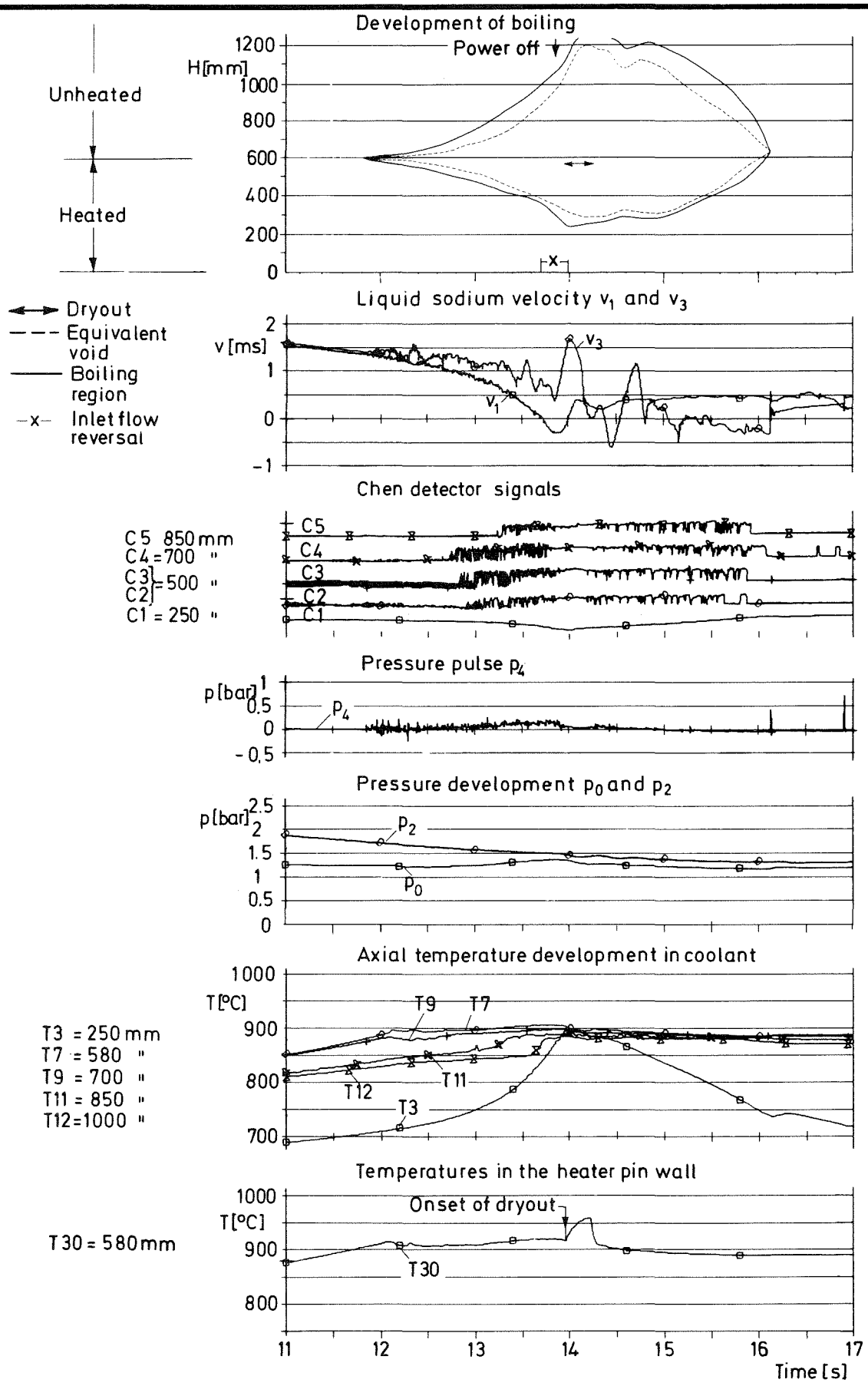

GfK IRE	7-Pin Bundle, Pump Run Down Results of Test 7-2/14	Fig. 21

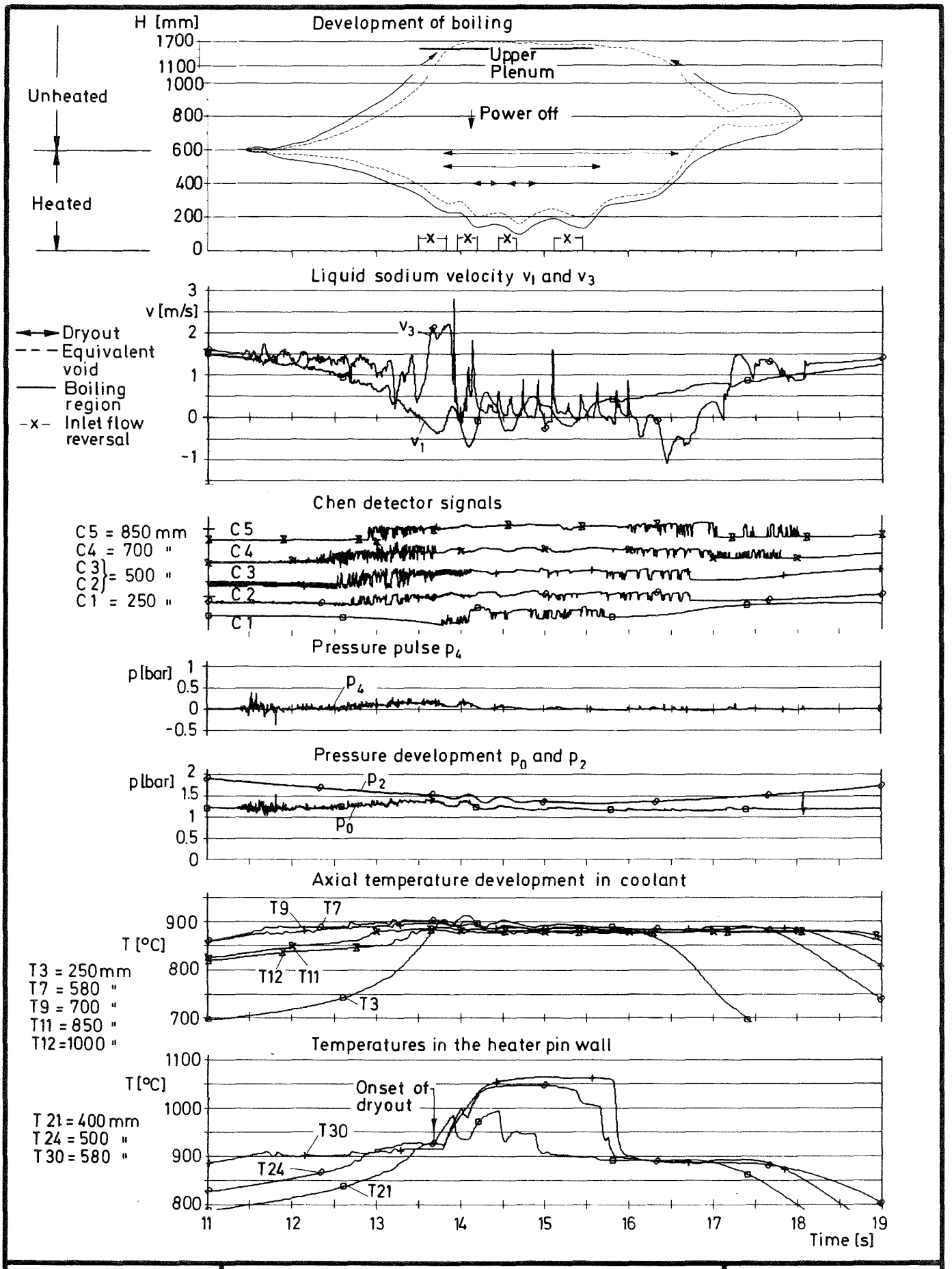

GfK IRE	7-Pin Bundle, Pump Run Down Results of Test 7-2/25	Fig. 22

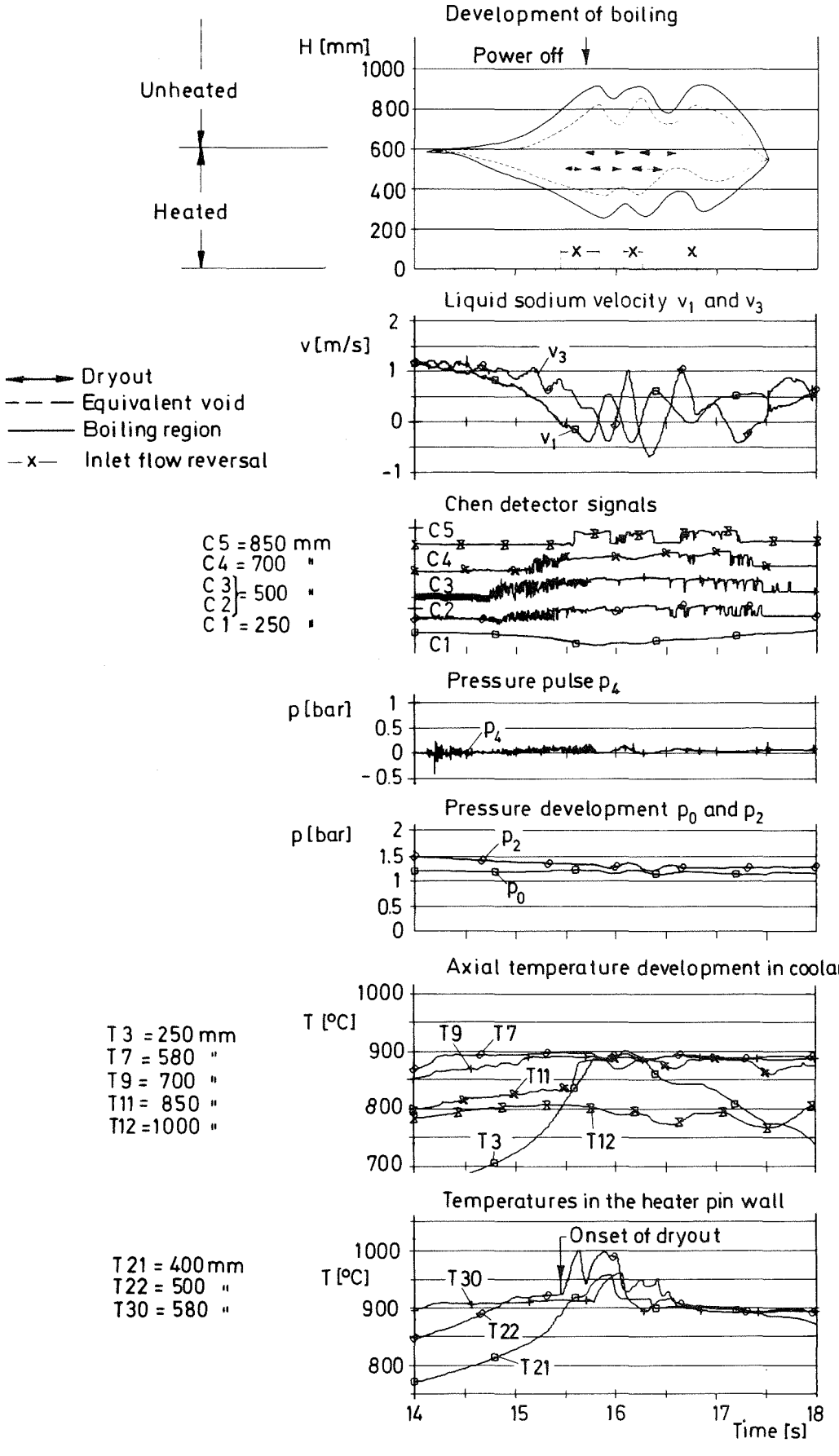

GfK IRE	7-Pin Bundle, Pump Run Down Results of Test 7-2/17	Fig. 23

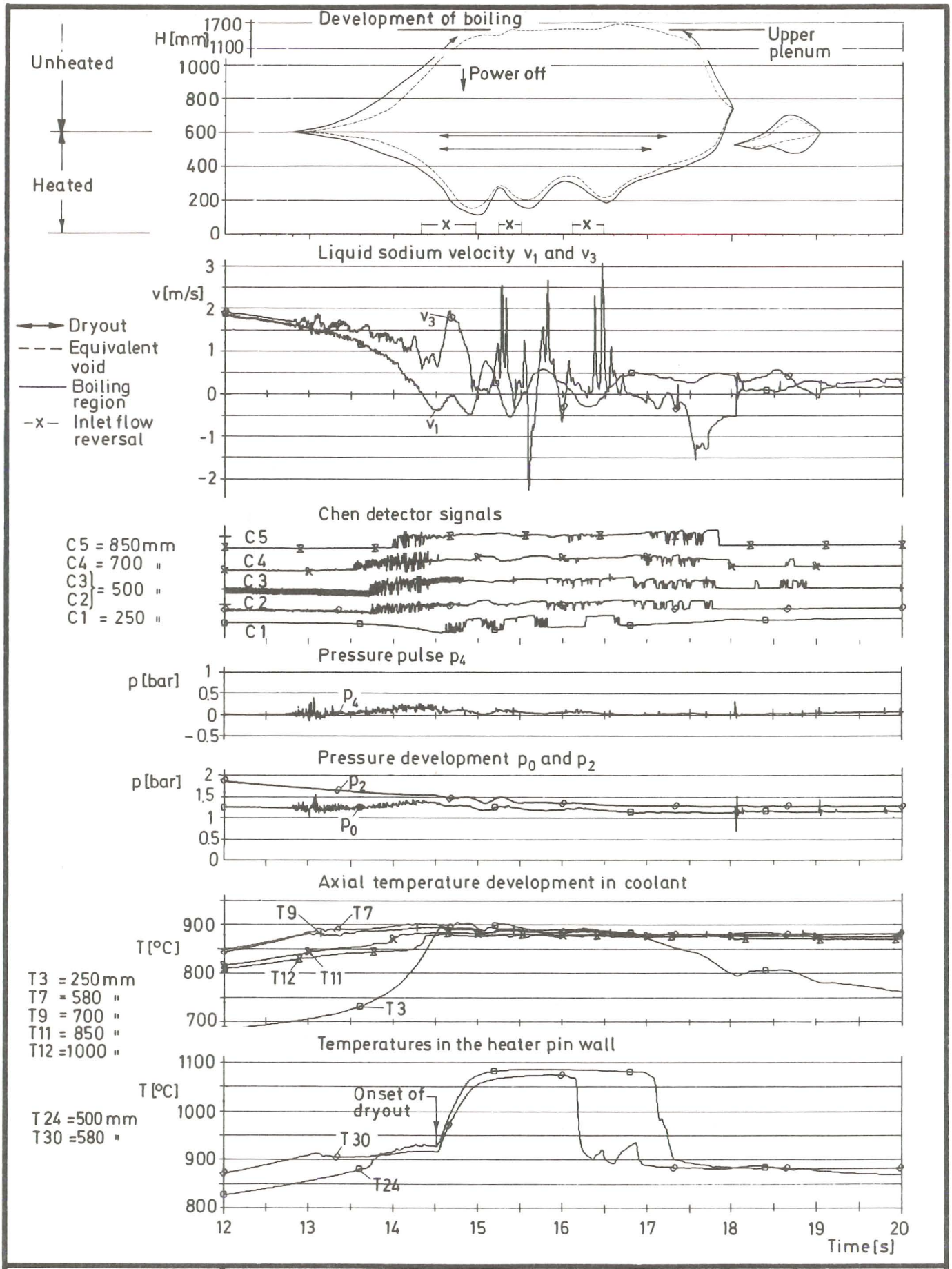

GfK IRE	7-Pin Bundle, Pump Run Down Results of Test 7-2/27	Fig. 24

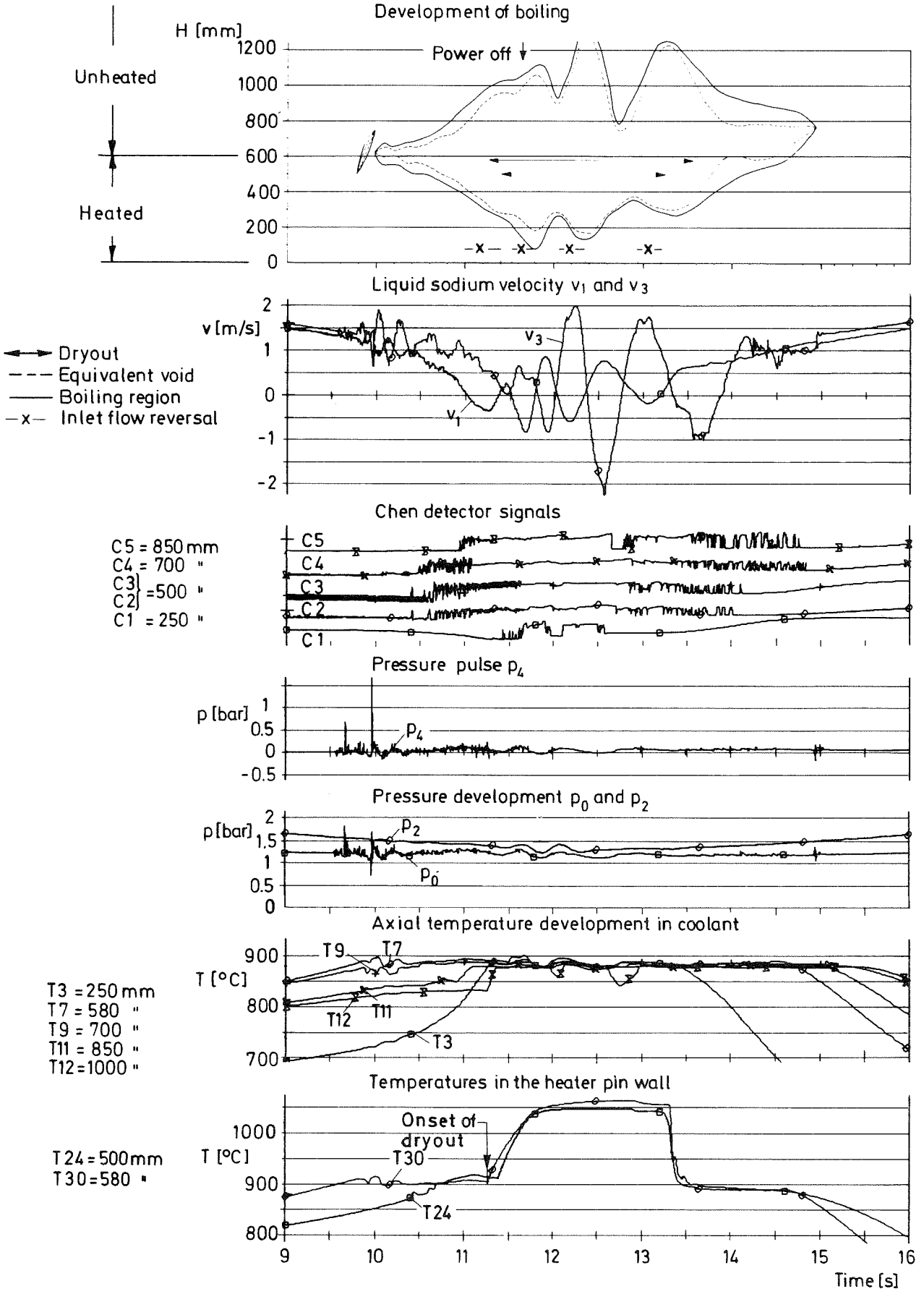

GfK IRE	7-Pin Bundle, Pump Run Down Results of Test 7-2/22	Fig. 25

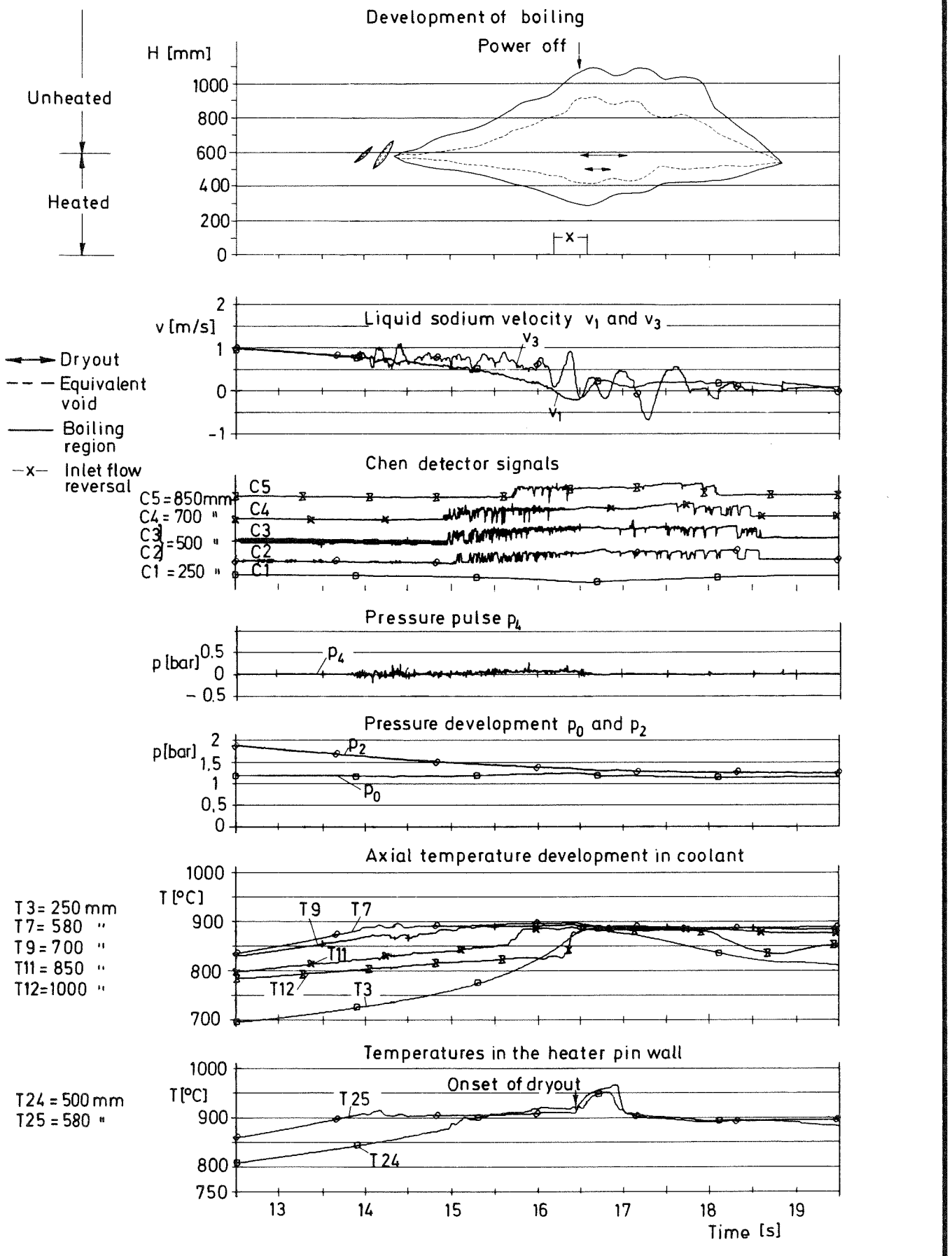

GfK IRE	7-Pin Bundle, Pump Run Down Results of Test 7-2/13	Fig. 26

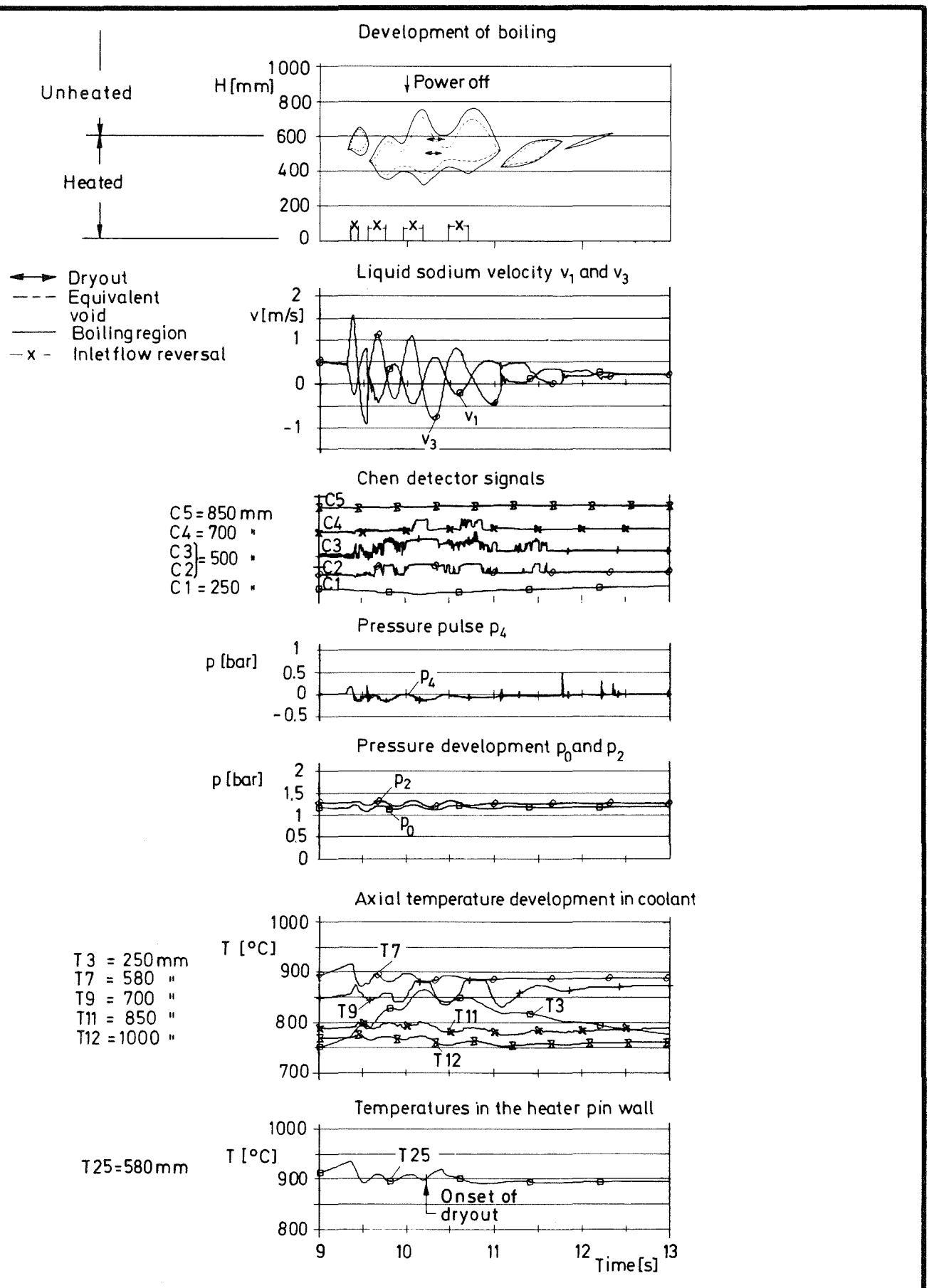

GfK IRE	7-Pin Bundle, Pump Run Down Results of Test 7-2/15	Fig. 27

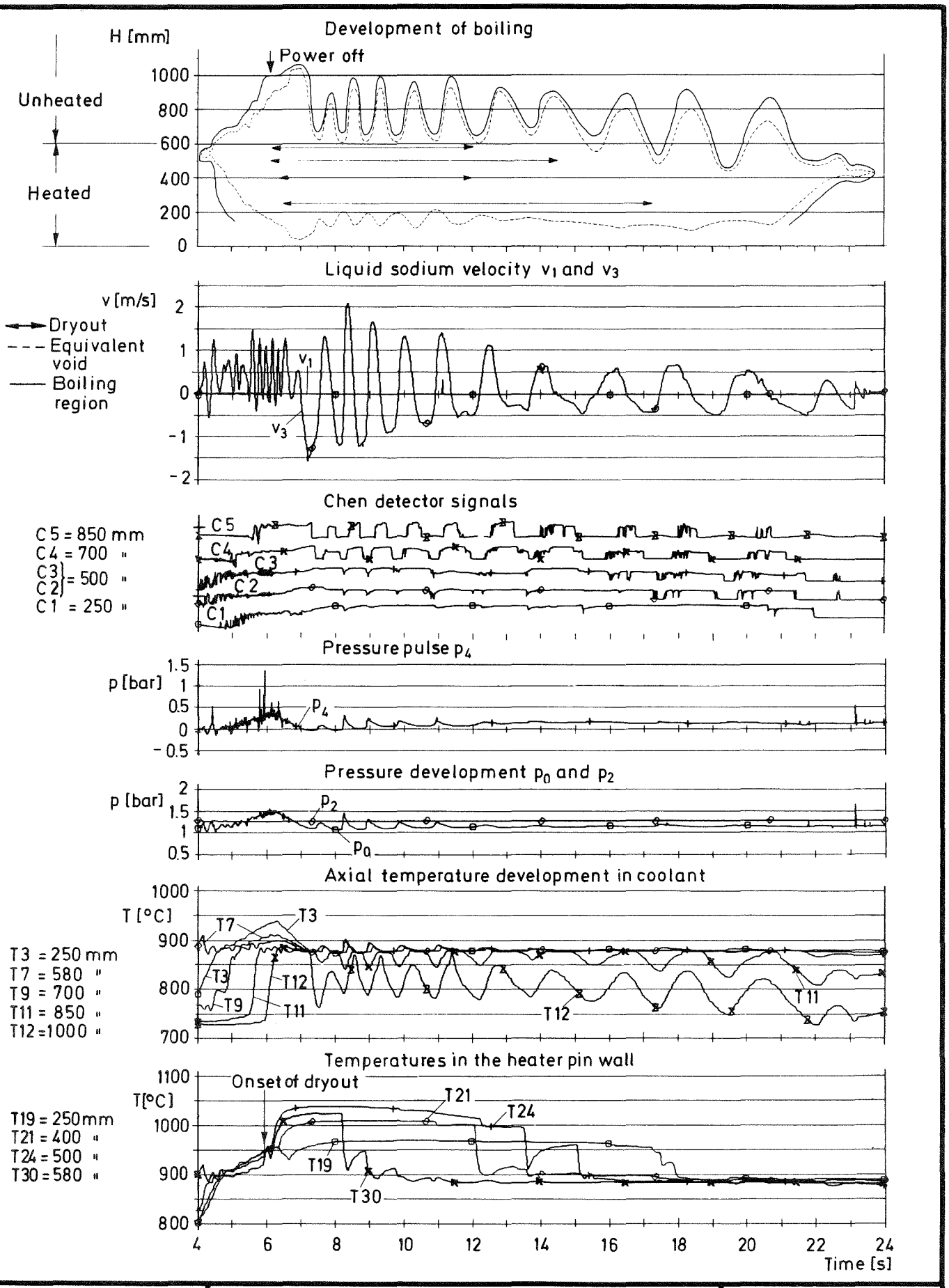

GfK IRE	7-Pin Bundle, Pump Run Down Results of Test 7-2/28	Fig. 28

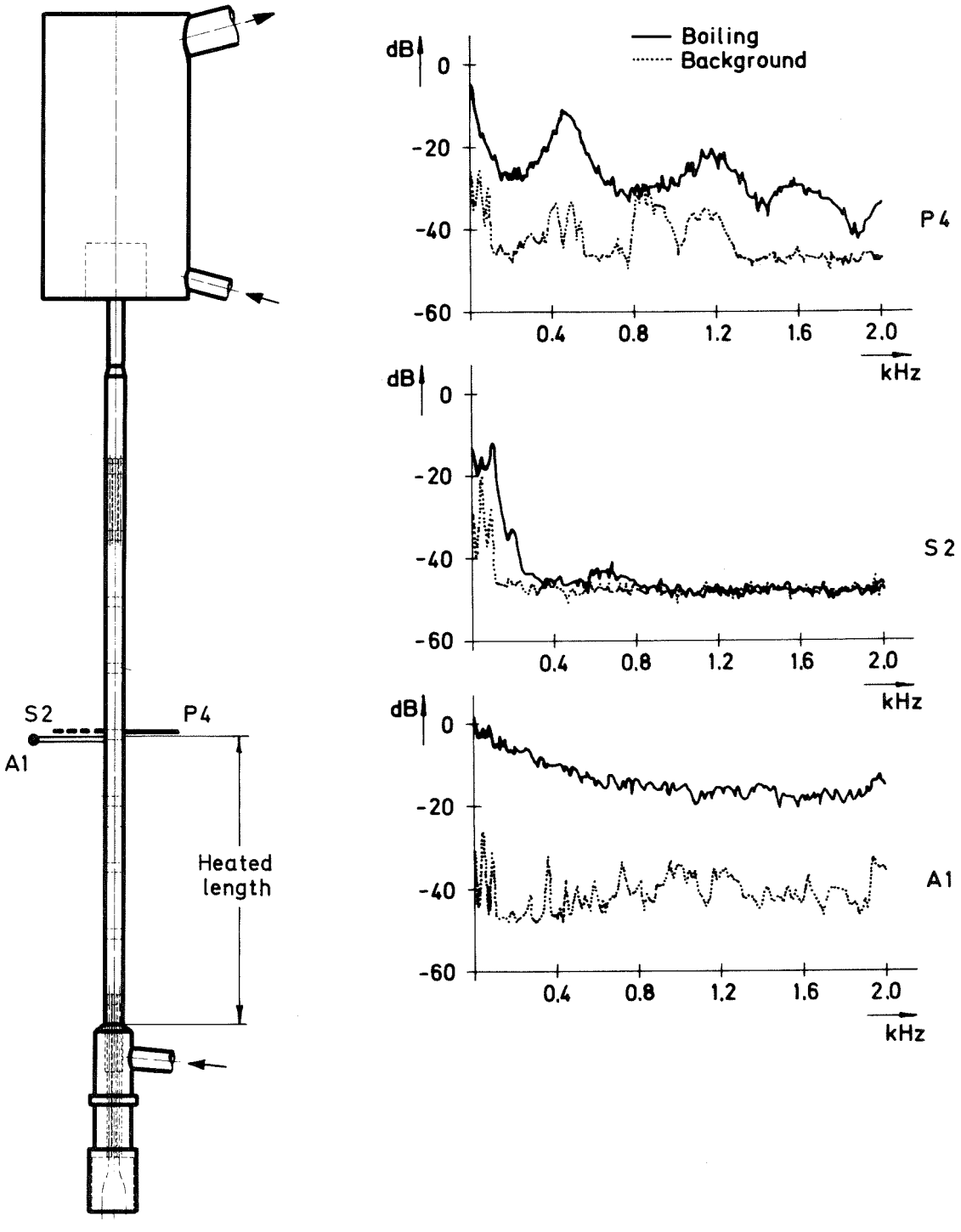

GFK IRE	7-Pin Bundle Test 7-2/25 Comparison of Autocorrelated Boiling Spectra	Fig. 29

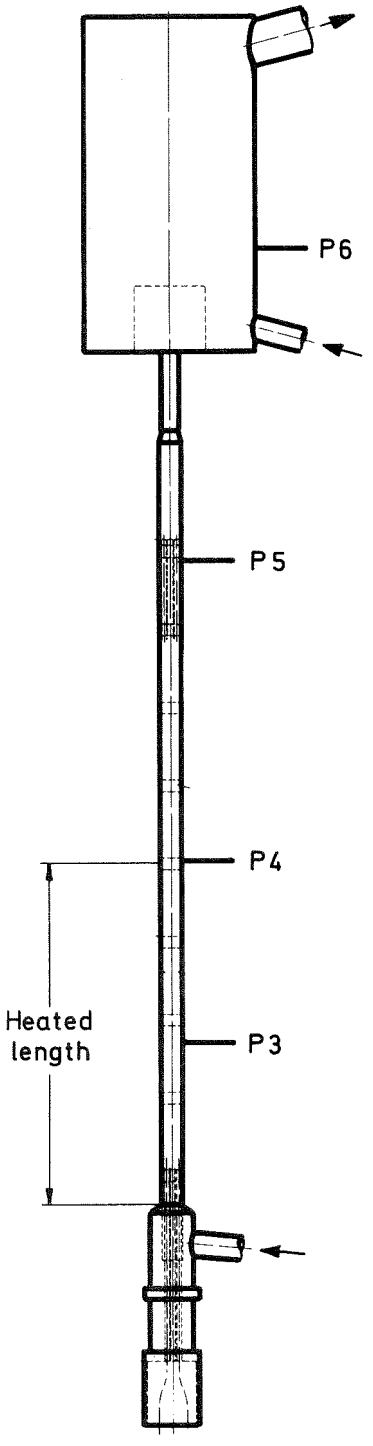

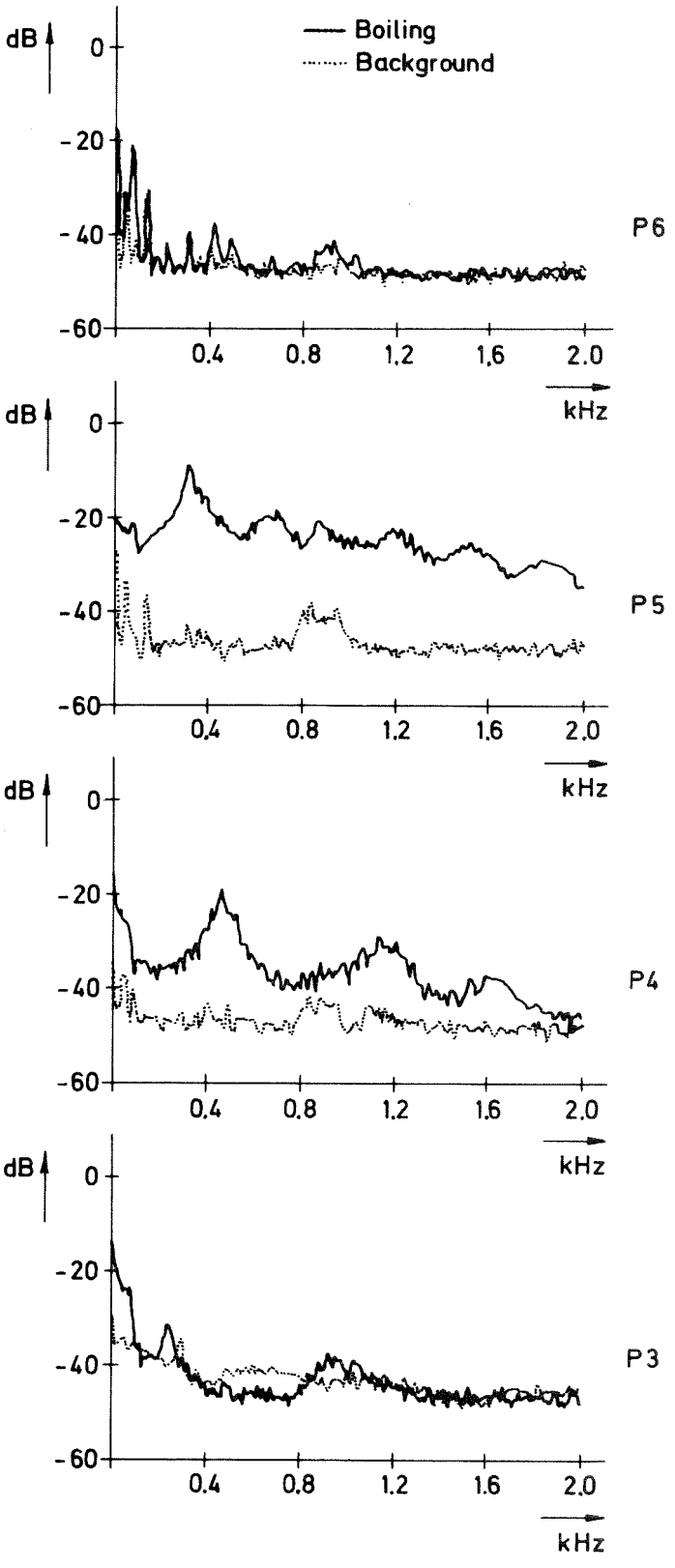

GFK IRE	7-Pin Bundle Test 7-2/25 Autocorrelated Pressure Spectra at Different Axial Levels	Fig. 30

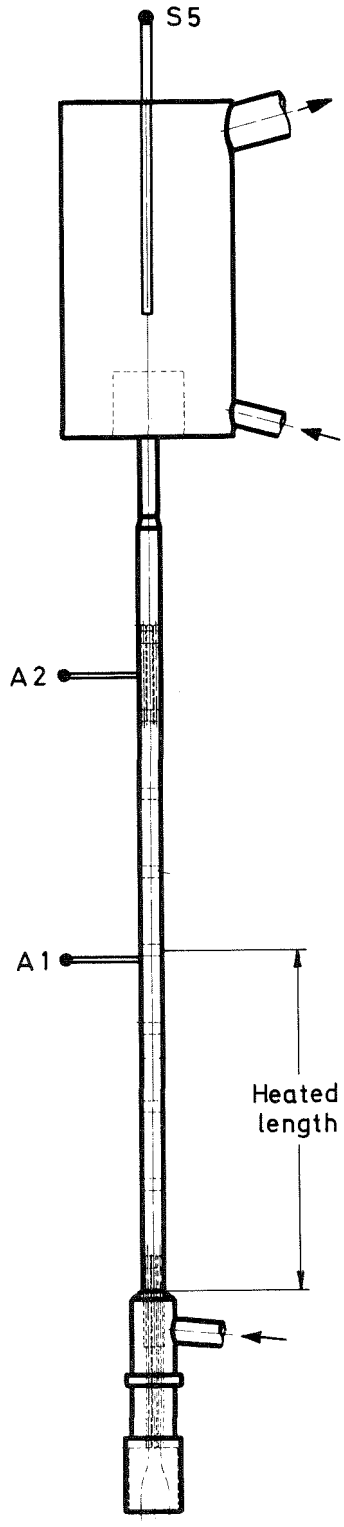

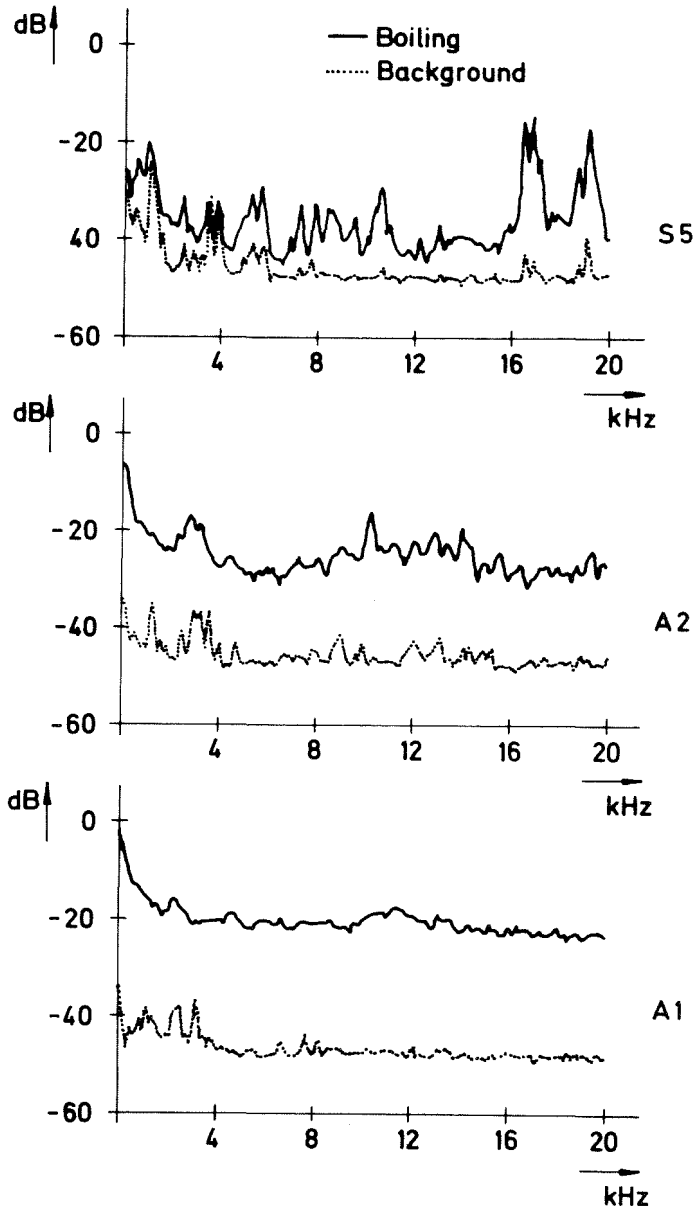

GFK IRE	7-Pin Bundle Test 7-2/25 Autocorrelated Acoustic Spectra at Different Axial Levels	Fig. 31

Conditions at the onset of boiling:

	7-Pin bundle	annulus
ΔT_s [k]	68	34
v_1 [m/s]	0.33	1.1
Δp [bar]	0.201	0.2
ϕ [W/cm²]	99.3	123
P_{syst} [bar]	1.05	0.785
Run No	7-2/24	16/14

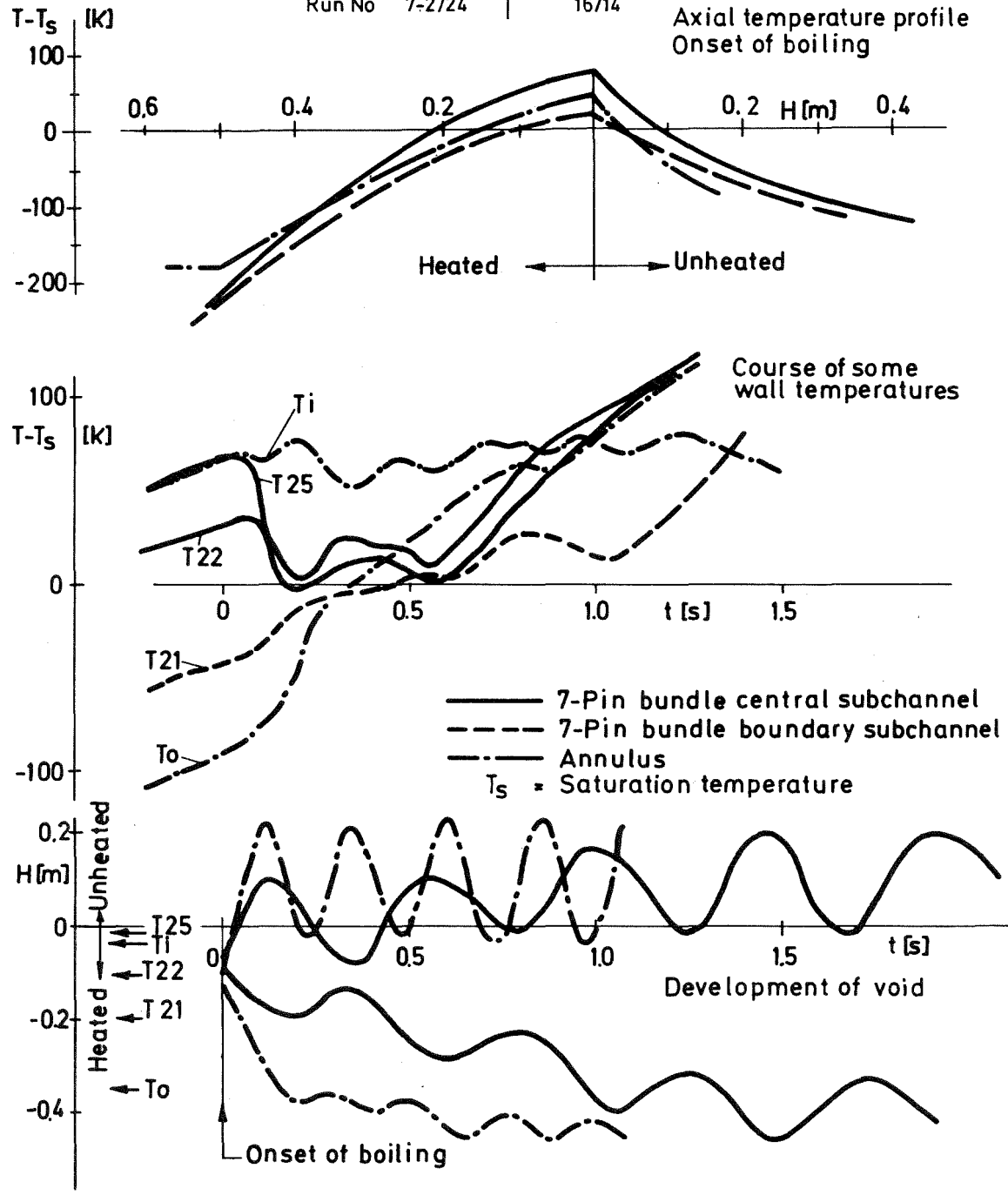

GfK IRE	Comparison of Boiling Processes in 7-Pin Bundle and Annular Geometry	Fig. 32

SUMMARY TABLE

	Test No. 7-2/	13	14	15	16	17	22	24	25	27	28
STEADY STATE	Channel Outlet Pressure (bar)	1.052	1.052	1.052	1.520	1.053	1.053	1.053	1.053	1.053	1.053
	Channel Inlet Pressure (bar)	3.85	3.88	2.00	4.18	4.00	2.79	2.03	3.80	3.90	2.19
	Pressure Drop(bar)	2.80	2.83	0.95	2.66	2.95	1.74	0.98	2.75	2.85	1.14
	Throttle Valve Setting (1)	C	B	A	B	A	A	A	B	A	D
	Flow Velocity (m/sec)	2.05	3.20	2.10	3.00	4.00	3.11	2.15	3.10	4.02	3.02
	Heat Flux (w/cm^2)	98.2	149.8	98.3	150.3	170.8	153.7	99.3	153.5	177.5	152.6
	Inlet Temperature (^oC)	563	562	562	562	483	559	553	559	559	559
	Outlet Temperature (^oC)	723	723	725	735	625	730	715	730	709	730
NUCLEATION	Time Transient Begins t_t (sec)	4.80	2.75	3.75	3.15	2.90	3.40	3.50	3.40	3.70	3.02
	Time Boiling Begins t_B (sec)	13.88	11.85	9.30	12.15	14.15	9.59	9.87	11.42	12.80	3.97
	$t_B - t_t$ (sec)	9.08	9.10	5.55	9.00	11.25	6.19	6.37	8.02	9.10	0.95
	Channel Inlet Pressure at t_B (bar)	1.65	1.72	1.28	2.12	1.48	1.55	1.25	1.82	1.23	1.26
	Mean Rate of Inlet Pressure Change (bar/sec)	-.243	-.235	-.130	-.230	-.224	-.201	-.122	-.247	-.305	Rapid
	Pressure at End of Heated Section at t_B(bar)	1.18	1.24	1.16	1.72	1.20	1.20	1.13	1.21	1.23	1.12
	Total Pressure Drop at t_B (bar)	.60	.67	.23	.60	.43	.50	.21	.77	.18	-
	Flow Velocity at t_B (m/sec)	.76	1.4	.42	1.13	1.12	1.41	.33	1.48	1.70	0
	Superheat (^oC)	0	0	22	0	0	0	68	0	0	27
BOILING	Length Equivalent Void t_B + 1 (mm)	55	125	not	115	135	115	not	120	150	310
	Length Boiling Region t_B + 1 (mm)	140	220	com-	215	240	210	com-	205	300	600
	Length Equivalent Void t_B + 1.5 (mm)	130	285	par-	265	355	440	par-	290	470	465
	Length Boiling Region t_B + 1.5 (mm)	300	445	able	425	545	560	able	420	590	800
	Lower Interface Reaches 300 mm (sec+t_B)	2.28	2.03	"	1.97	1.56	1.63	"	2.15	1.72	0.54
	Upper Interface Reaches 850 mm (sec+t_B)	1.65	1.42	"	1.52	1.46	1.37	"	1.45	1.20	1.62
	Flow Reversal Begins (sec+t_B)	2.32	1.85	.04	1.80	1.33	1.43	.01	2.06	1.53	-
	Dryout Begins (sec+t_B)	2.62	2.09	0.89	1.98	1.38	1.51	.57	2.25	1.75	1.96
	Equivalent Film Thickness (mm) (based on heat flux and time to dry out)	0.90	1.08	0.31	1.03	0.81	0.81	0.20	1.24	1.07	1.03
	Power Off (sec+t_B)	2.62	2.00	0.69	2.06	1.57	2.08	1.34	2.69	2.02	2.27
	Boiling Ceases (sec+t_B)	4.98	4.30	1.76	4.12	3.39	5.37	5.75	6.63	5.24	19.6

(1) A - fully open, no throttling B - intermediate C - almost closed, high throttling D - closed